Received: 9 December 2018 | Revised: 19 March 2019 | Accepted: 25 March 2019

DOI: 10.1002/joc.6080

RESEARCH ARTICLE

International Journal of Climatology RMetS

Backward and forward drift trajectories of sea ice in the northwestern Arctic Ocean in response to changing atmospheric circulation

Ruibo Lei[1] | Dawei Gui[1,2] | Jennifer K. Hutchings[3] | Jia Wang[4] | Xiaoping Pang[2]

[1]SOA Key Laboratory for Polar Science, Polar Research Institute of China, Shanghai, China

[2]Chinese Antarctic Center of Surveying and Mapping, Wuhan University, Wuhan, China

[3]College of Earth Ocean and Atmospheric Sciences, Oregon State University, Corvallis, Oregon

[4]Department of integrated physical and ecological modeling and forecasting, National Oceanic and Atmospheric Administration Great Lakes Environmental Research Laboratory, Ann Arbor, Michigan

Correspondence
Ruibo Lei, SOA Key Laboratory for Polar Science, Polar Research Institute of China, 451# Jinqiao Road, Shanghai 200136, China.
Email: leiruibo@pric.org.cn

Funding information
National Key R&D Program of China, Grant/Award Numbers: 2018YFA0605903, 2016YFC14003; National Natural Science Foundation of China, Grant/Award Number: 41722605; National Science Foundation, Grant/Award Numbers: OPP1722729, OPP1740768

Abstract

To track sea ice motion, four ice-tethered buoys were deployed at 84.6°N and 144.3°W, 87.3°N and 172.3°W, 81.1°N and 157.4°W, and 82.8°N and 166.5°W in summers of 2008, 2010, 2014, and 2016, respectively. In addition, the remote sensed ice motion product provided by National Snow and Ice Data Center was used to reconstruct backward and forward ice drifting trajectories from the buoy deployment sites during 1979–2016. Sea ice in the central Arctic Ocean in late summer is trending to have travelled from lower latitudes, and to be advected to the region more involved in the Transpolar Drift Stream (TDS) during 1979–2016. The strengthened TDS has played a crucial role in Arctic sea ice loss from a dynamic perspective. The trajectory of ice is found to be significantly related to atmosphere circulation indices. The Central Arctic Index (CAI), defined as the difference in sea level pressure between 84°N, 90°W and 84°N, 90°E, can explain 34–40% of the meridional displacement along the backward trajectories, and it can explain 27–40% of the zonal displacement along the forward trajectories. The winter Beaufort High (BH) anomaly can explain 18–27% of the zonal displacement. Under high positive CAI values or high negative winter BH anomalies, floes from the central Arctic tended to be advected out of the Arctic Ocean through Fram Strait or other marginal gateways. Conversely, under high negative CAI values or high positive winter BH anomalies, ice tended to become trapped within a region close to the North Pole or it drifted into the Beaufort Gyre region. The long-term trend and spatial change in Arctic surface air temperature were more remarkable during the freezing season than the melt season because most energy from the lower troposphere is used to melt sea ice and warm the upper ocean during summer.

KEYWORDS

Arctic, atmospheric circulation pattern, climate change, drifting trajectory, motion, sea ice

1 | INTRODUCTION

In the Arctic amplification of climate warming (Screen and Simmonds, 2010), the extent and thickness of Arctic sea ice have declined dramatically in recent decades (Parkinson and Comiso, 2013; Lindsay and Schweiger, 2015), which dominated the sea ice loss at the global scale although the Antarctic sea ice extent shows a contrasting trend to increase

This is an open access article under the terms of the Creative Commons Attribution License, which permits use, distribution and reproduction in any medium, provided the original work is properly cited.

© 2019 The Authors. International Journal of Climatology published by John Wiley & Sons Ltd on behalf of the Royal Meteorological Society.

(Simmonds, 2015). The Arctic amplification is not uniform for the whole troposphere. The ratio of the Arctic near-surface warming to that of the whole tropospheric column is highest in autumn (Screen and Simmonds, 2010). The time of onset of ice surface melt and refreezing, determined by satellite passive microwave measurements, have shown that the Arctic-wide melt season has lengthened at the rate of 5 days/decade during 1979–2013, primarily because of delayed autumn freeze-up (Stroeve et al., 2014). The lengthened melting season resulted in the increase in melt pond coverage over the ice, which exhibits a slight upward trend of 2.4% from 2000 to 2011 (Rösel and Kaleschke, 2012).

Sea ice moves in response to ocean currents, wind stress, and the Coriolis force, as well as the effects of sea surface slope and internal ice stress (Tremblay and Mysak, 1997). The Arctic winds generate an anticyclonic circulation system in the Canadian Basin, that is, the Beaufort Gyre (BG), with average clockwise ice motion in the western Arctic Ocean; and a cyclonic circulation with its centre in the Laptev Sea or Barents Sea (Proshutinsky and Johnson, 1997). The Transpolar Drift Stream (TDS) flows between these two circulation cells, transporting sea ice from the north of Siberia toward Fram Strait. The BG and TDS are not isolated and their boundary is ambiguous because of regulation by the atmospheric circulation patterns (Kwok et al., 2013). The Beaufort High (BH) forces the oceanic BG (Proshutinsky et al., 2009). Collapse of the BH with anomalous low sea level air pressure (SLP) could result in an anomalous reversal of the normally anticyclonic surface winds and ice motion in the western Arctic (Moore et al., 2018). The circulation pattern of the BG is closely related to the seasonality of synoptic processes (Asplin et al., 2009). The collapse of the BH was more ubiquitous during summer when the frequencies of Arctic cyclone increases in the central Arctic, in contrasting to the lower Arctic cyclone activity during winter (Simmonds et al., 2008). However, during recent winters, more cyclonic activity extended from Barents Sea into the central or the western Arctic Ocean (Rudeva and Simmonds, 2015), which resulted in the collapse of the BH and the reversal of the BG (Asplin et al., 2009; Moore et al., 2018; Petty, 2018). The cyclonic activities also would lead to more moist intrusions into the Arctic, which is projected to increase in a warming climate (Screen et al., 2018). During these intrusions the near-surface air temperature (SAT) in the region close to the North Pole has risen above freezing point even during winters (Graham et al., 2017). On the other hand, both the reversal of BG and the enhanced positive polarity of the Arctic Dipole Anomaly (DA) can accelerate the northward advection of sea ice from the BG region into the TDS region (Asplin et al., 2009; Wang et al., 2009). During the reversals of BG, the ice from the BG can be advected northeastward into the TDS (Lukovich and Barder, 2006); while the enhanced positive DA tends to transport the ice from the BG to the TDS through the western boundary of BG (Wang et al., 2009).

Increase in air temperature and melt pond coverage over the ice can effectively reduce the ice strength at the floe scale by increasing the brine and pore volumes within the ice cover (Timco and Johnston, 2002), while the drastic decline in ice thickness and concentration is hypothesized to weaken the ice strength at the basin scale (Hutter et al., 2018). The decreases in ice strength might result in enhanced Arctic sea ice mobility and increase its vulnerability to the storms. Storms coupled with increasing fetch because of the decreased ice concentration generate large waves which can propagate into the pack ice, thereby causing of the flexural swell and failure of sea ice (Asplin et al., 2012 and 2014; Thomson and Rogers, 2014). This process fragments floes, which then more responsive to oceanic and atmospheric forcings and more susceptible to lateral melting. Numerical modelling of Arctic sea ice (Zhang et al., 2012) has shown that a decline in ice volume during the period 2007–2011 results in a 37% decrease in ice mechanical strength and a reduction of 31% in internal ice force, which in turn leads to increases in ice speed (13%) and deformation rates (17%) in comparison with the 1979–2006 mean, particularly in the western Arctic because there has been a rapid depletion of thicker, older ice. Zhang et al. (2012) stressed that, while model studies can shed light on the changes in the dynamic properties of Arctic sea ice, it is important to monitor the changes through satellite and in situ observations because the fundamental knowledge used for numerical modelling is largely based on a system dominated by thick, multi-year ice. Satellite data have confirmed that the spatially averaged drift speed within the Arctic Basin increased by $10.6 \pm 0.9\%$ decade^{-1} between 1992 and 2009 (Spreen et al., 2011). Sea ice motion is an important factor determining summer ice retreat in the Arctic Ocean due to redistribution of ice mass (Ogi et al., 2010; Kimura et al., 2013). Climate modelling results suggest that ice export through the Fram Strait can explain 28% of variance in long-term trends of sea ice thickness over the Arctic Ocean (Langehaug et al., 2013). Sea ice outflow through Fram Strait is regulated primarily by the east–west dipole pattern of SLP anomalies with centres of action located over the Barents Sea and Greenland (Tsukernik et al., 2010).

The most significant decline in summer Arctic sea ice extent has occurred in the sector stretching from Beaufort Sea to East Siberian Sea (Petty et al., 2016). However, sea ice area within this sector has substantial interannual variability attributable to the atmospheric circulation (Vihma et al., 2012; Petty et al., 2016). This sector of Arctic Ocean is the major investigation region of the Chinese National Arctic Research Expeditions in summers of 2008, 2010,

2014, and 2016. During these cruises, ice camps were established in the northwestern Arctic Ocean at 84.6°N and 144.3°W, 87.3°N and 172.3°W, 81.1°N and 157.4°W, and 82.8°N and 166.5°W, respectively (Figure 1). Considering the climatological mean ice drift, these sites are located in the boundary region between the BG and the TDS (Petty et al., 2016). To identify the source and destination of sea ice in this region can help to thoroughly understand the mass exchange of sea ice between the systems of BG and TDS, which may further influence sea ice loss in the entire Arctic Ocean. The drift trajectories of ice floes are crucial not only from a climatological perspective, but also provides context for determining pollutant migration over the Arctic Ocean. For example, the polymer composition of microplastics deposited in sea ice depends significantly on the drift paths of the sea ice (Peeken et al., 2018).

In this study, a satellite-derived product of daily ice motion vectors was used to identify the year to year changes in the backward and forward trajectories of ice drifting from the ice camps during 1979–2016 and their responses to changes in the atmospheric circulation pattern. The SAT derived from the reanalysis data and sea ice concentration derived from passive microwave remote sensing were used to explore the changes in climate and ice conditions along the trajectories, and their association with the variance of sea ice advection.

2 | DATA AND METHODS

At each ice camp, one sea Ice Mass balance Buoy (IMB; Richter-Menge et al., 2006) was deployed to track ice drift and to measure the seasonal evolution of ice mass balance. The IMB was equipped with a Navman Jupiter 32 global position system (GPS) receiver and it sampled positional data hourly with the horizontal accuracy better than ±10 m. The operational period of each IMB deployed in August 2008 and 2010 was approximately 11 months, while the operational period of the IMBs deployed in August 2014 and 2016 lasted longer than 1 year.

The Polar Pathfinder 25-km EASE-grid sea ice motion vectors dataset version 3 (Tschudi et al., 2016), available from the National Snow and Ice Data Center (NSIDC), provides Arctic sea ice drift vectors from October 1978 to February 2017. The sea ice drift vectors are obtained through calculating the correlation of groups of pixels between satellite image pairs and merging with both buoy drift vectors obtained from the International Arctic Buoy Program and the reanalyzed wind data from the National Centers for Environmental Prediction/National Center for Atmospheric Research (NCEP/NCAR). The NSIDC ice drift vectors were used to reconstruct the backward and forward trajectories of the ice camp deployment sites for the period from August 1979 to August 2016. This ice motion product was selected to be used for the following reasons. (a) It allows identification of the long-term change of sea ice kinematics because it covers a more extensive time period than other products, for example, those from the Centre ERS d'Archivage et de Traitement (CERSAT; Girard-Ardhuin and Ezraty, 2012) and the Ocean and Sea Ice Satellite Application Facility (OSI-SAF; Lavergne and Eastwood, 2010). (b) It covers all seasons, which is beneficial for constructing continuous trajectories. (c) It has better temporal (daily) and spatial (25 km) resolutions compared with the CERSAT and

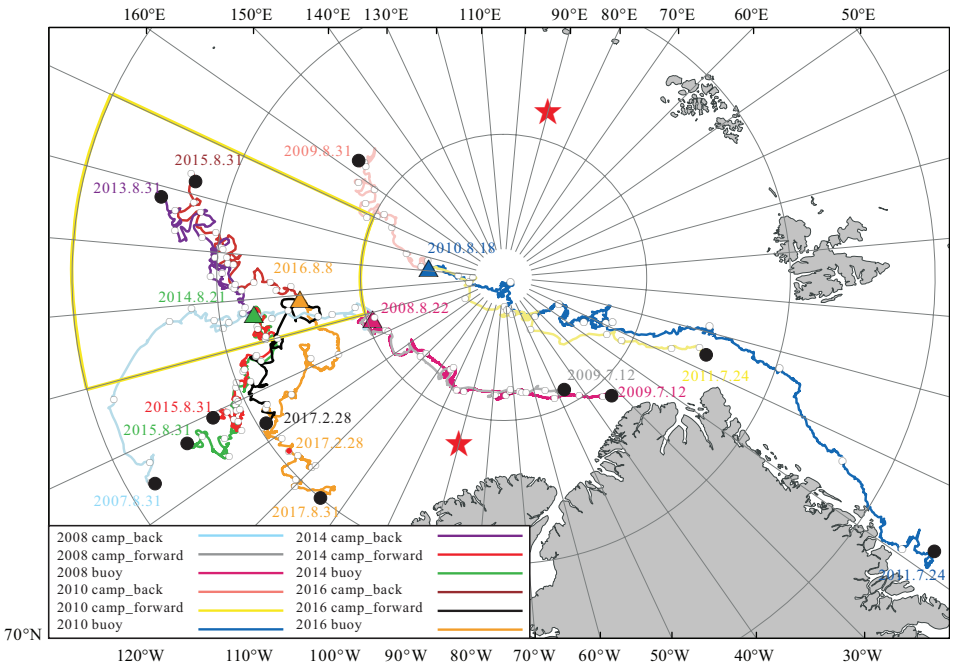

FIGURE 1 Deployment sites of the CHINARE ice camps (triangles) and the trajectories of the buoys deployed at the camps. Also shown are the backward (to 31 August of the previous year) and forward (to 31 August of the following year or to the end of the buoy operation) trajectories estimated using the NSIDC product. Open and solid circles denote the monthly positions and terminal points of a trajectory, respectively. Red stars show the locations where the SLP was used to calculate the CAI. The solid yellow sector indicates the climatological domain of the BH defined by Petty et al. (2018)

OSI-SAF products. (d) Its uncertainty is comparable with the OSI-SAF product and smaller than the CERSAT product (Sumata et al., 2014).

To reconstruct the forward trajectories, we projected the initial positions of the camps to the same Cartesian coordinate system as used by the NSIDC ice motion vectors, which is centred on the North Pole with the Y axis following the Greenwich meridian and the horizontal resolution of 25 km. The zonal and meridional coordinates of the initial camp site are $X(0)$ and $Y(0)$, with the ice drift vectors at time t along the ice trajectories are $U(t)$ and $V(t)$. The zonal and meridional coordinates of the reconstructed ice trajectories at the time t were calculated as:

$$X(t) = X(t-1) + U(t-1) \cdot \delta t \tag{1}$$

$$\text{and } Y(\mathrm{t}) = Y(t-1) + V(t-1) \cdot \delta t, \tag{2}$$

where the δt is the calculation time step (1 day). Finally, the reconstruct ice trajectory in the Cartesian coordinate was reprojected back to geographic coordinates. The procedure to reconstruct the backward trajectories was the same as that for the forward trajectories but using a negative time step. The terminal points of the reconstructed backward and forward trajectories were set on 31 August of the previous year and the following year relative to the time of deployment of the buoys, respectively. This cutoff date was defined to make the study period close to 1 year for both backward and forward trajectories. Due to data gaps in the NSIDC ice motion product, the ice trajectories in the ice season 1992/93 and 1993/94 cannot be reconstructed. Using the data from August 1979 to August 2016, we reconstructed 280 ice trajectories in total for four camp sites. Among these cases, there were seven for which the reconstructed forward trajectories did not reach the defined cutoff date because the trajectory reached the ice edge prior to the cutoff time. These trajectories were eliminated from further statistical analysis. Comparison of the actual buoy drift trajectories and estimated forward trajectories showed good agreement in terms of the general direction and destination (Figure 1); hence, we have confidence in applying the NSIDC ice vectors to reconstruct the drift trajectories camps would have experienced in other years.

Changes in atmosphere and sea ice conditions during 1979–2016 along the fixed backward and forward trajectories were obtained by interpolation of the ERA-Interim reanalysis (Dee et al., 2011) 2-m SAT and multichannel microwave radiometer - special sensor microwave imager sounders (SMMR-SSMIS) sea ice concentration retrieved using the National Aeronautics and Space Administration Team algorithms (Markus and Cavalieri, 2000) onto the trajectories. The fixed backward and forward trajectories were reconstructed in the year of buoy operation. Several methods have been used to define the ice melt season based on the ice surface condition (Stroeve et al., 2014), the ice concentration (Parkinson, 2014), or the SAT (Lei et al., 2018). In this study, to investigate the climate change, the onset dates of melt and freezing points in early summer and autumn were identified using the reanalysis SAT. Following Lei et al. (2018), the melt and freezing points were set as 0°C corresponding to the melt of snow or surface near-fresh ice and −1.8°C corresponding to the freeze-up of seawater, respectively. Due to its synoptic-scale variability, generally associated with the cyclonic activities (Simmonds et al., 2008; Simmonds and Keay, 2009), the SAT falls below −1.8°C in autumn and rises above 0°C in early summer several times. To account for this, the onset dates were defined as the dates when the running mean SAT in a given temprol window was over −1.8 or 0°C. Šmejkalová et al. (2016) used a 31-day sliding temporal window to characterize lake-ice phenology for the circumpolar Arctic regions. For time series used in this study, the window of 10 days is the shortest window which can avoid the running mean SAT passing across the threshold temperature repeatedly. Changing the length of the sliding window from 10 to 30 days leads to variance in the onset dates of melt or freezing season of less then 3 days, which implifies the onset date is not very sensitive to the window size. Hence, we used the modest length of 20 days for the sliding window to identify the onset dates of melt or freezing seasons. Long-term changes in average SAT in the freezing and melt seasons were then obtained. The freeze-up period in the Arctic is among the windiest and stormiest time of the year (Sotiropoulou et al., 2016). The strong winds would induce the wind-wave driven fractures of the new ice, creating pancakes. Consequently, the stormy conditions can delay the thickening of the new ice; however, this does not preclude the possibility of freeze up occurring during relatively quiescent periods between storms. Thus, the freezing onset date identified using SAT can indicate atmospheric surface cooling that preceds and occurs during freeze-up. However, the threshold of −1.8°C cannot indicate the onset of basal freezing for multiyear ice because of the thermal inertia exerted by snow and ice. Taking the 2010 camp as an example, the basal ice melt of the 1.49-m ice covered by 0.15-m of snow ceased by October 16, 2010 when the 20-day running mean SAT fell below −11°C (Lei et al., 2018). Thus, the isotherm date of −11°C, defined as the time when the 20-day running mean SAT fell below −11°C, was used as an estimate for the onset of basal ice freezing. Choosing an SAT threshold for freezeup is somewhat arbitrary because the onset of basal freezing also depends on the thicknesses of snow and ice and on the heat flux from the upper ocean. Changing the threshold SAT from −7 to −15°C leads to the variance of 24 days for the isotherm date. However, the long-term trends of the isotherm dates based on the thresholds from −7 to −15°C reveal the same pattern as found for the isotherm date using −11°C.

For example, along the forward trajectory from the 2008 camp site, the isotherm dates corresponding to the thresholds ranging from −7 to −15°C have the long-term trends within a narrow range from 2.8 to 3.2 days/decade during 1979–2016. This gives us further confidence to use a constant threshold of air temperature for all study sites. Moreover, it is convenient to identify the spatiotemporal change in atmosphere forcing for ice growth by using a constant threshold.

To quantify the change in ice conditions, this study focused on the September average ice concentration along the September leg of the backward trajectories. This was because the central Arctic Ocean was covered by compact sea ice with less interannual variability in ice concentration in other months. To explore the influence of sea ice advection on the atmospheric thermodynamic forcing and ice conditions along the trajectories, we also calculated the average SAT in the freezing season and the September ice concentration along the backward trajectories obtained for the years 1979–2016. We focused on the backward trajectories because the geographical locations of these trajectories can be depicted using the latitude to a great extent (Figure 2), and because the meridional variance of Arctic atmospheric forcing and ice conditions are generally larger than their zonal variance. The statistical relationships between average SAT in the freezing season or the average September ice concentration against the average latitude of the trajectories were then obtained.

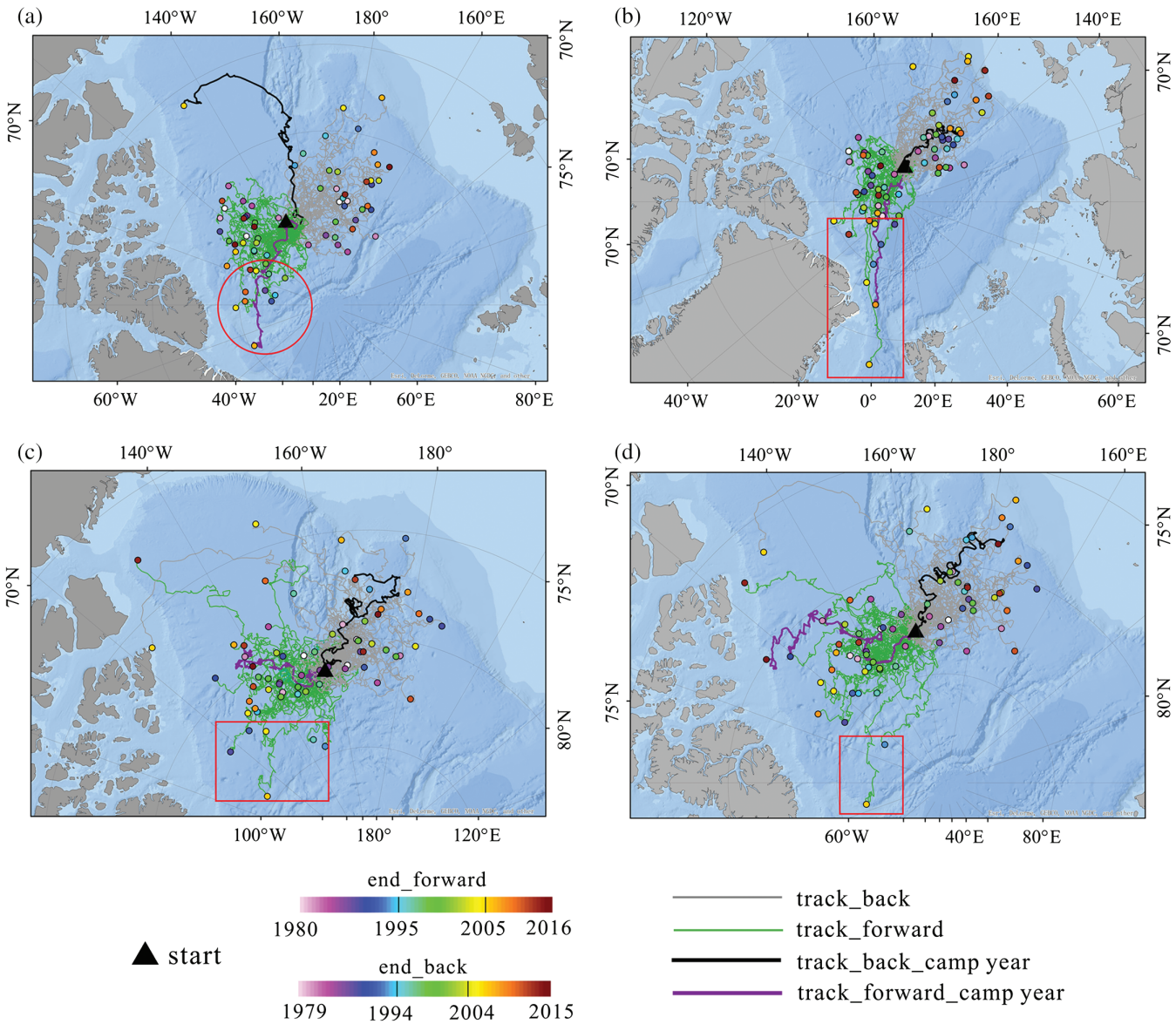

FIGURE 2 Estimated backward (light grey line) and forward (light green line) trajectories using the NSIDC data in the years 1979–2016 for ice drifting from the camp sites of 2008 (a), 2010 (b), 2014 (c), and 2016 (d). Solid coloured circles denote terminal points of the trajectories by 31 August. Thick lines denote estimated trajectories obtained in the operational years of the buoys. Red rectangle or circle depicts the terminal points of the forward trajectories that were clearly advected into the TDS region

To quantify the regulating effect of the atmospheric circulation patterns on the sea ice motion, we calculated the seasonal Arctic Oscillation (AO) and DA indices, as well as the monthly Central Arctic Index (CAI) and BH anomaly. The SLP data of the NCEP/NCAR reanalysis (Kalnay et al., 1996) north of 70°N were used to derive the empirical orthogonal function modes, of which the AO and DA are the first and second modes (Wang et al., 2009). The CAI, which was defined as the difference in SLP between 84°N, 90°W and 84°N, 90°E as shown in Figure 1, was calculated using the European Centre for Medium-Range Weather Forecasts ReAnalysis (ERA)-Interim reanalysis data according to Vihma et al. (2012). We used the CAI, but not the east–west SLP gradient between the Barents Sea and Greenland as in Tsukernik et al. (2010), because we wanted to characterize the overall magnitude of ice motion through the TDS, not just for the region across the Fram Strait. The BH anomaly was calculated as the spatial average SLP anomaly over the domain of 75°–85°N, 170°E–150°W relative to the 1979–2016 mean using the ERA-Interim reanalysis data. This domain, as shown in Figure 1, was defined according to Moore et al. (2018).

Long-term trends of atmospheric patterns and ice records during 1979–2016 were determined using linear regression. Correlation analysis was employed to test the statistical relationships between pairs of parameters. However, some variables, for example, the latitude of reconstructed trajectory, the SAT, and the ice concentration, are expected to have a long-term trend. It is hard to distinguish the physically dependence and the long-term covariation when performing the correlation analysis on the raw data. To address this issue we also recalculated the regressions using the detrended data if the long-term trend of the raw data was significant at the 95% level. The level of significance of the trends and correlations was evaluated using a two-tailed *t* test.

3 | RESULTS

3.1 | Interannual changes in the reconstructed ice trajectories

In the years 1979–2016, ice floes at the 2008 camp site were advected mainly from the Makarov Basin along the TDS, with a few cases moving from the Canadian Basin along the western boundary of the BG (Figure 2a). The CAI can explain 39% ($p < .001$) of the interannual variance of latitude of the original positions, that is, the meridional displacement along the backward trajectories (Figure 3a). According to the reconstructed backward trajectory, the floe was advected rapidly westward along the southern boundary of BG in September–November 2007. This was consistent with the fact that the westward transport of sea ice during summer–autumn in the southern BG region was relatively high in 2007 compared with the 1979–2016 mean because of anomalous anticyclonic winds in the BG region (Petty et al., 2016). In the southern BG region, the rapid westward transport of sea ice was sustained into winter and spring of the 2007/08 ice season. This led to a large amount of sea ice in this region being advected to the East Siberian Sea, which further resulted in rapid retreat of the sea ice in the Beaufort Sea during the 2008 melt season because of the lack of thick multi-year ice (Kimura et al., 2013). The 2008 camp floe had drifted northward from December 2007 until it reached the site of the ice camp. Starting from the camp site, the floe moved gradually away from the BG region and it drifted eastward across the Lomonosov Ridge into the Lincoln Sea by July 2009. This was the only case of an ice floe from the camp site drifting to this region during 1979–2016. The average value of the CAI (DA index) from December 2007 to August 2009 was 3.8 hPa (0.55), which was the first (third) highest during 1979–2016, indicating a strong TDS. Thereby, the floe drifted almost parallel to the direction of the TDS during this period.

Close inspection of the estimated ice trajectories showed the terminal positions of the forward trajectories depended mainly on the direction of ice motion in winter (December–February), because the ice floes originated from the camp sites would generally drift to the intersection region between the northeast of BG system and the downstream TDS region by that time. In those ice seasons (22 cases) in which the ice originating from the 2008 camp site clearly drifted into the BG region, the average winter AO index had negative polarity (−0.13) and the average winter BH anomaly was positive (3.6 hPa). Both characteristics can be related to enhanced anticyclonic motion of the sea ice in the western Arctic (Vihma et al., 2012; Moore et al., 2018). In those ice seasons (11 cases within red circles in Figure 2a) in which the ice clearly drifted into the TDS region, the average winter AO index had positive polarity (0.68) and the average winter BH anomaly was negative (−6.5 hPa). Both of these characteristics can be related to the enhanced cyclonic motion of sea ice in the western Arctic. The winter AO index or the winter BH anomaly can explain 16% ($p < .05$) or 27% ($p < .01$), respectively, of the variance of longitude of the terminal positions of the forward trajectories, that is, the zonal ice advection (Figure 4a). An enhanced TDS could have promoted advection of the ice floe from the 2008 camp site into the TDS region. The increased values of the CAI ($p < .01$; Figure 3e) and DA ($p < .05$) might be related to the lower longitude of the terminal positions by regulating the zonal ice advection, meaning the ice floe was advected into the TDS regions.

The ice camp of 2010 was located near the central axis of the TDS (Figure 2b). Thus, the reconstructed backward and

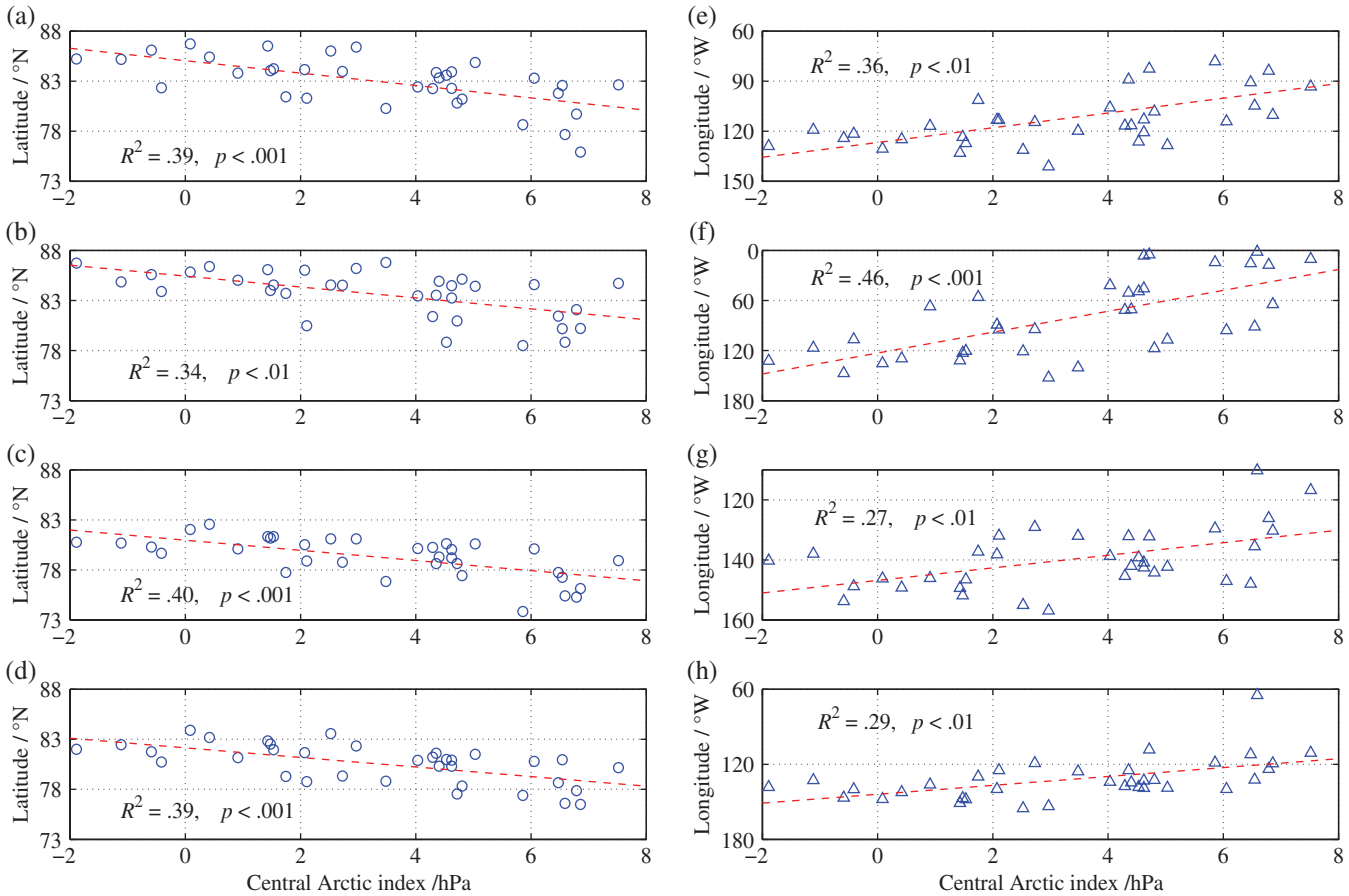

FIGURE 3 Statistical relationship between latitude of the original positions of backward trajectories (a–d) or longitude of the terminal positions of forward trajectories (e–h) from the camp sites of 2008, 2010, 2014, and 2016 against the CAI during 1979–2016

forward trajectories during 1979–2016 were influenced primarily by the intensity of the TDS. The floes originated mainly from the northern East Siberian Sea or the Makarov Basin. The CAI can explain 34% ($p < .01$) of the variance in latitude of the original positions (Figure 3b). However, no significant relationship was identified between the DA index and the latitude of the original positions. When the TDS was strengthened or when the BH was abnormally negative, the ice floes from the camp site tended to drift into the TDS region toward the Fram Strait; otherwise, they would be trapped within a region close to the North Pole or drifted into the BG region. The CAI and DA values can explain 46% ($p < .001$; Figure 3f) and 14% ($p < .05$), respectively, of the variance in longitude of the terminal positions. The average CAI value was 6.0 hPa for those cases in which the ice clearly drifted into the TDS region (13 cases within the red rectangle in Figure 2b). This value is much larger than the 1979–2016 average (0.33 ± 0.25 hPa). The winter AO index or the winter BH anomaly can explain 15% ($p < .05$) or 24% ($p < .01$), respectively, of the variance of the terminal positions of the forward trajectories (Figure 4b).

In comparison with earlier years, the sites of the ice camps of 2014 and 2016 were deployed at relatively low latitudes, that is, 81.10 and 82.75°N, respectively (Figure 2c, d). The CAI can explain 40% ($p < .001$; Figure 3c) and 39% ($p < .001$; Figure 3d) of the variance of latitude of the original positions of backward trajectories corresponding to the 2014 and 2016 camp sites, respectively. In addition, the BH anomaly can explain 17% ($p < .05$) and 18% ($p < .05$) of the variance of longitude of the original positions of the backward trajectories corresponding to the 2014 and 2016 sites, respectively. This indicates the backward trajectories were influenced primarily by the TDS and only slightly by the BG system. Starting from the sites of these two camp sites, the floes tended to drift within the BG region for most years during 1979–2016. Only six and two cases during 1979–2016 showed clear advection of ice floes into the TDS system from the 2014 and 2016 camp sites, respectively. The CAI can explain 27% ($p < .01$; Figure 3g) and 29% ($p < .01$; Figure 3h) of the variance in longitude of the terminal positions for the 2014 and 2016 sites, respectively. The winter AO index and the winter BH anomaly can explain 19% ($p < .01$) or 20% ($p < .01$; Figure 4c),

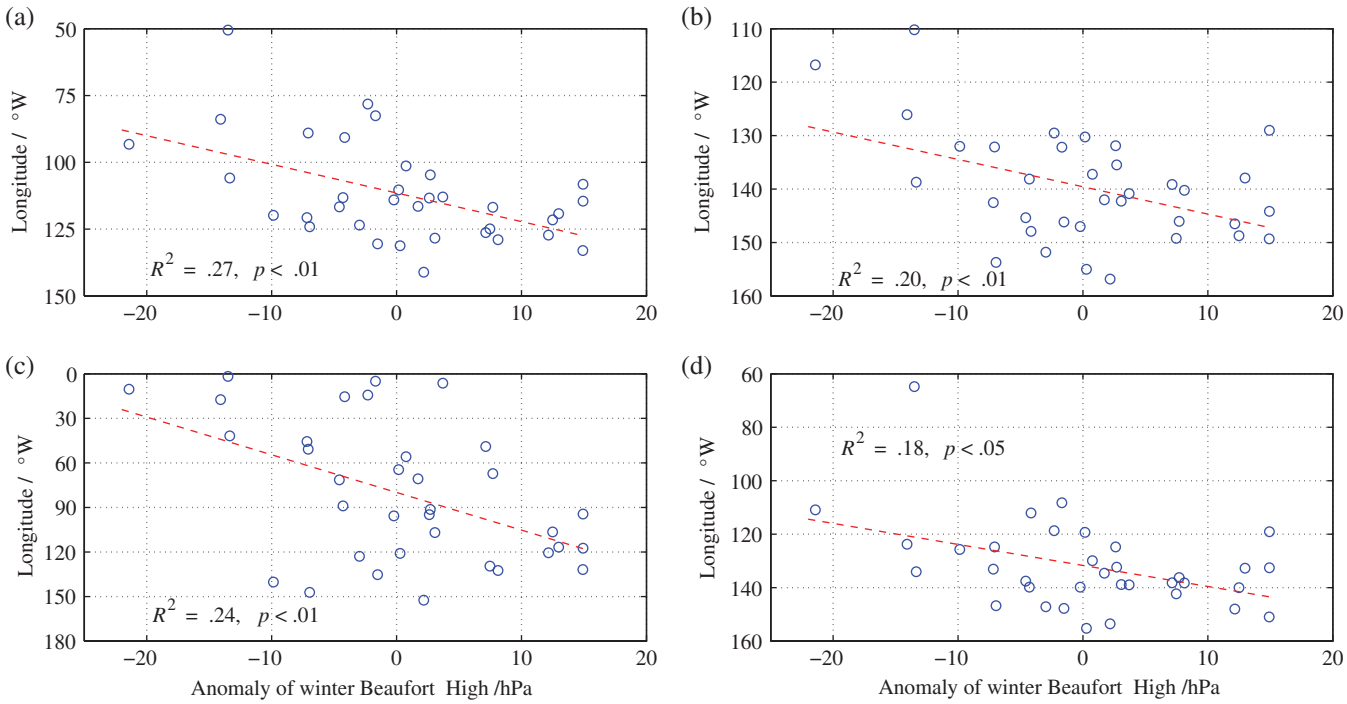

FIGURE 4 Statistical relationship between longitude of terminal positions of forward trajectories from the camp sites of 2008 (a), 2010 (b), 2014 (c), and 2016 (d) against winter BH anomaly during 1979–2016

respectively, of the variance in longitude of the terminal position for the 2014 site, and 14% ($p < .05$) or 18% ($p < .05$; Figure 4d), respectively, for the 2016 site. Because the CAI was defined as the difference in SPL between 84°N, 90°W and 84°N, 90°E, increased cyclonic activities in the Barents and Kara seas would increase the magnitude of the CAI; otherwise, an increase in cyclonic activities over the Canadian Arctic Archipelago would decrease the CAI. For example, during January–March 2017, there was a long-lasting low system that occurred in the Barents Sea, which enhanced the cyclonic circulation and resulted in the highest CAI (8.6 hPa) over the period of 1979–2017. This low system tended to extend into the Chukchi and Beaufort seas, shrinking in the direction toward the Canadian Arctic Archipelago (Moore et al., 2018; Petty, 2018). Thus, it also leads to the lowest BH anomaly for 1979–2017. Both the regimes of positive CAI and negative BH facilitated the ice advection from the BG system to the TDS. The buoy deployed at the camp 2016 drifted from 80.1°N and 132.9°W to 80.7°N and 119.9°W, which implied the influence of cyclonic activities on the atmospheric circulation index, and furthermore on the ice motion.

From 1979 to 2016, the original positions of all deployment sites showed significant tendency to be advected from lower latitudes. This was significant at the 99% (95%) confidence level for the 2008 and 2010 (2014 and 2016) sites. Furthermore, the ice floes from all sites were advected toward lower-longitude regions from 1979 to 2016 ($p < .05$), that is, toward the region closer to Fram Strait. This indicates that ice floes from the sectors of the Chukchi and East Siberian seas have tended to be advected into the central Arctic Ocean and subsequently into Fram Strait in recent years. Furthermore, the frequently occurring positive polarity of DA during recent summers would be likely to lead to the anomalous advection of warm air from the south and the flow of relatively warm waters from the North Pacific into the Arctic Ocean, reduced cloudiness and enhanced insolation, in addition to increased sea ice export, which could result in reduced Arctic sea ice extent, especially in the Pacific sector of Arctic Ocean (Wang et al., 2009; Overland et al., 2012; Lei et al., 2016). Therefore, during recent summers, the ice has retreated early in the Chukchi and East Siberian seas, which is conducive to the accessibility of Arctic Northeast Passage (Lei et al., 2015).

3.2 | Climate change along ice trajectories

From the SAT interpolated along the estimated trajectories during 1979–2016, it was found that the onset dates of melt and freeze did not show significant difference among the trajectories, apart from one exception for the forward trajectory from the 2010 site that occurred early on 6 June (Figure 5 and Table 1). This was because the ice from this site was advected southward to the Fram Strait. The long-term average of the onset dates of the melt determined using the SAT for the backward (forward) trajectories was 10–12 June (6–12 June), while the long-term average of the onset dates of the freezing determined using the SAT for the forward

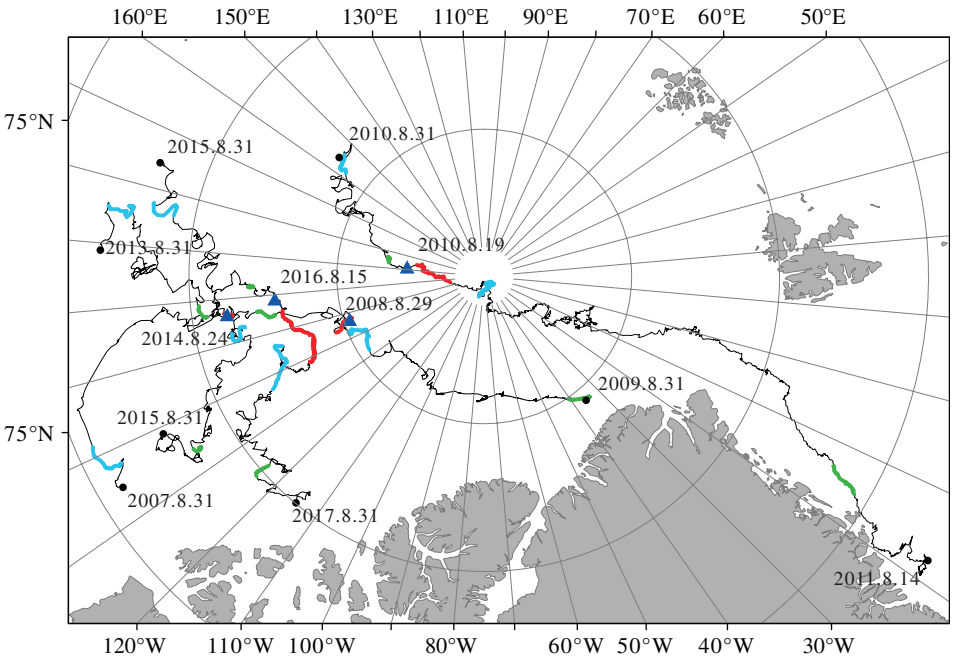

FIGURE 5 Trajectories (black lines) from 31 August in years prior to the buoy deployments to 31 August in years after buoy deployments. The backward and forward trajectories prior to or after the operational lives of the buoys were estimated using the NSIDC ice motion product. Note that the forward trajectory after August 14, 2011 could not be estimated because the ice had been advected to the ice edge. Blue triangles indicate deployment locations of camps. The red, light blue, and green thick lines denote trajectories for the corresponding average date (±*SD*) in 1979–2016 when SAT falls below −1.8 and −11°C and rises above 0°C, respectively

trajectories was 26–28 August. They did not show any significant long-term trend for any ice camp site. This is different from the long-term trend of surface freeze-up identified from satellite passive microwave measurements, which was about 10 and 8 days/decade during 1979–2013 in the Chukchi and East Siberian seas, respectively (Stroeve et al., 2014). Thus, the significant delays in autumn surface freeze-up were mainly attributed to the ice-albedo feedback, but not the changes in autumn SAT. The increase in melt pond coverage over the ice during the summer also would enhance the ice-albedo feedback and facilitates the delayed freeze-up of ice surface (Lei et al., 2016). For the open water, the strengthened cyclonic activities during the summer and early autumn (e.g., Simmonds and Keay, 2009) also would promote the delayed freeze-up through inducing ocean vertical mixing (Rainville and Woodgate, 2009). The insignificant spatiotemporal change in the onset dates of freezing and melt points determined using the SAT implies that the poleward gradient for surface atmospheric thermodynamic forcing is weak during summer, and that the loss of summer Arctic sea ice cannot generate significant positive feedback for warming of the surface atmosphere over the ice zone. The melting of sea ice during summer would consume heat from the atmosphere, resulting in the SAT remaining near 0°C, which restricts local warming for the Arctic ice zone in summer. This mechanism was termed as the effect of water-ice bath by Overland (2009). However, we suggest that summer warming in the central Arctic would be promoted once the ice-free region extended further northward into the central Arctic, because the ice-free region has reasonably weak ability to regulate feedbacks related to air temperature increase compared with the ice zone.

Based on the onset dates of freeze and melt, we defined the melt and freezing seasons as persisting from 12 June to 28 August and from 1 September to 6 June, respectively. The mean SAT in the melt season ranged from 0.5 to 1.0°C and did not show significant spatial variance among the estimated trajectories. The spatial variance of the SAT in the freezing season was relatively larger compared with the melt season. Its value obtained from the forward trajectories ranged from −18.6 to −20.6°C, which was slightly lower than that obtained from the backward trajectories (−18.2 to −19.0°C), with the exception for the 2010 camp. This exception can be explained by the fact that the forward trajectories from the 2010 site were located at relatively low latitudes compared with the other sites. The isotherm dates of −11°C along the forward trajectories were earlier than along the backward trajectories for all cases by 5–8 days, which indicates that the SAT during early autumn in regions north of the Canadian Arctic Archipelago and Greenland was lower than in regions north of the Beaufort, Chukchi, and East Siberian seas. Furthermore, the long-term trends toward earlier isotherm dates of −11°C were more significant along the backward trajectories than along the forward trajectories (Figure 6). From the linear regression, the −11°C isotherm dates were delayed by 15–23 days from 1979 to 2016 along the backward trajectories, that is, much more than along the forward trajectories (11–14 days). This implies the onset of basal growth for the sea ice with the same thickness at low latitudes might be delayed further compared with the high-latitude pack ice zone. This mechanism, introduced by the warming SAT, would be strengthened by the ice-albedo feedback (Perovich et al., 2007), the increased downward longwave radiation because of the

TABLE 1 Averages of atmospheric parameters during 1979–2016 obtained along the fixed ice trajectories estimated in the operational years of the buoys, with the *SD* shown in parentheses

Trajectory	Downward crossing −1.8°C	Downward crossing −11°C	Upward crossing 0°C	SAT (12 Jun.–28 Aug.)/°C	SAT (1 Sep.–6 Jun.)/°C
Backward from 2008 camp	NaN	7 Oct. (10d)	12 Jun. (5d)	0.5 (0.3)	−18.8 (1.5)
Backward from 2010 camp	NaN	4 Oct. (10d)	12 Jun. (5d)	0.5 (0.4)	−19.0 (2.0)
Backward from 2014 camp	NaN	10 Oct. (11d)	10 Jun. (5d)	0.5 (0.3)	−18.2 (1.7)
Backward from 2016 camp	NaN	9 Oct. (11d)	11 Jun. (5d)	0.5 (0.3)	−18.7 (1.8)
Forward from 2008 camp	26 Aug. (5d)	1 Oct. (9d)	12 Jun. (4d)	1.0 (0.3)	−20.6 (1.4)
Forward from 2010 camp	27 Aug. (6d)	30 Sep. (9d)	6 Jun. (4d)	NaN	−18.6 (1.7)
Forward from 2014 camp	28 Aug. (5d)	2 Oct. (8d)	12 Jun. (4d)	0.6 (0.4)	−19.7 (1.4)
Forward from 2016 camp	26 Aug. (5d)	1 Oct. (8d)	14 Jun. (4d)	0.6 (0.4)	−20.3 (1.4)

strengthened poleward transport of moisture and the enhanced local evaporation from the leads (Lee et al., 2017), the increased heat flux transferring from the thin ice or leads (Screen and Simmonds, 2010), and the enhanced wave-induced break-up of the floes (Asplin et al., 2012 and 2014; Thomson and Rogers, 2014). Thereby, following northward expansion of the Marginal Ice Zone (MIZ) due to loss of Arctic sea ice in summer (Strong and Rigor, 2013), delayed onset of basal ice freezing would be exacerbated for the pan Arctic.

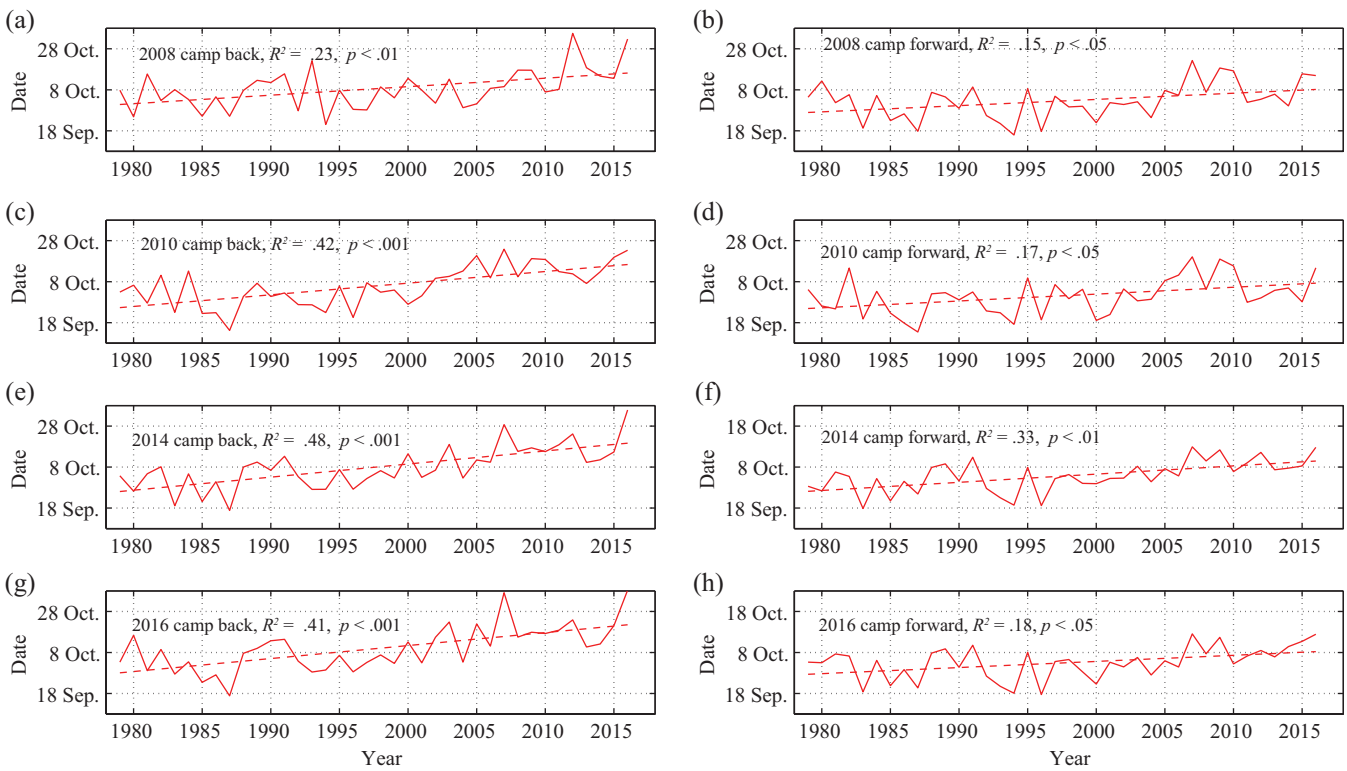

FIGURE 6 Long-term changes in the −11°C isotherm date obtained along the fixed backward (a–d) and forward (e–h) ice trajectories estimated in the operational years of the buoys

During the freezing season from 1 September to 6 June, SAT increased significantly during 1979–2016 along both backward and forward trajectories originating from all the deployment sites (Figure 7). The ERA-Interim reanalysis revealed that the trend of the SAT north of 70°N in 1989–2008 (Screen and Simmonds, 2010) was relative marked in autumn and winter (1.6°C per decade) compared to other seasons (0.5–0.9°C per decade). The near-surface warming amplification during autumn–winter is aided by strong low-level stability which limits vertical mixing through the troposphere (Overland, 2009) and increase in downward longwave radiation (Lee et al., 2017). Data obtained from land-based meteorological stations north of 70°N also showed that Arctic temperature amplification has been more remarkable in autumn and winter than in summer, with the rate of increase of SAT in autumn and winter being 1.9–2.5 times that in summer (Chylek et al., 2009). This highlights the importance of seasonal variability Arctic climate change. The long-term trends were more significant for backward trajectories than for forward trajectories. This indicates that air temperature warming during the freezing season in the Arctic Ocean was more remarkable at low latitudes than at high latitudes. In summer, low-latitude regions are more likely covered by low-concentration sea ice. The open water or thin sea ice in these regions tend to have a greater rate of ice growth during the freezing season. This can lead to increased heat flux from the ice-ocean system to the surface atmosphere and increased the evaporative moisture from the leads to the lower troposphere, both of which can produce enhanced local warming during the freezing season (Overland, 2009; Screen and Simmonds, 2010).

Along the estimated backward trajectories in various years, the average SAT in the freezing season was significantly dependent on the average latitude of the trajectories at the statistical level of 99.9% (Figure 8). Sea ice advected from lower latitudes experienced higher SATs during the freezing season. Because both the average SAT and the average latitude of the trajectories in the freezing season have a significant long-term trend at the 95% level, we recalculated the regressions using the detrended data. The detrended SAT in the freezing season can be explained by the detrended average latitude by 51, 48, 77, and 68% for

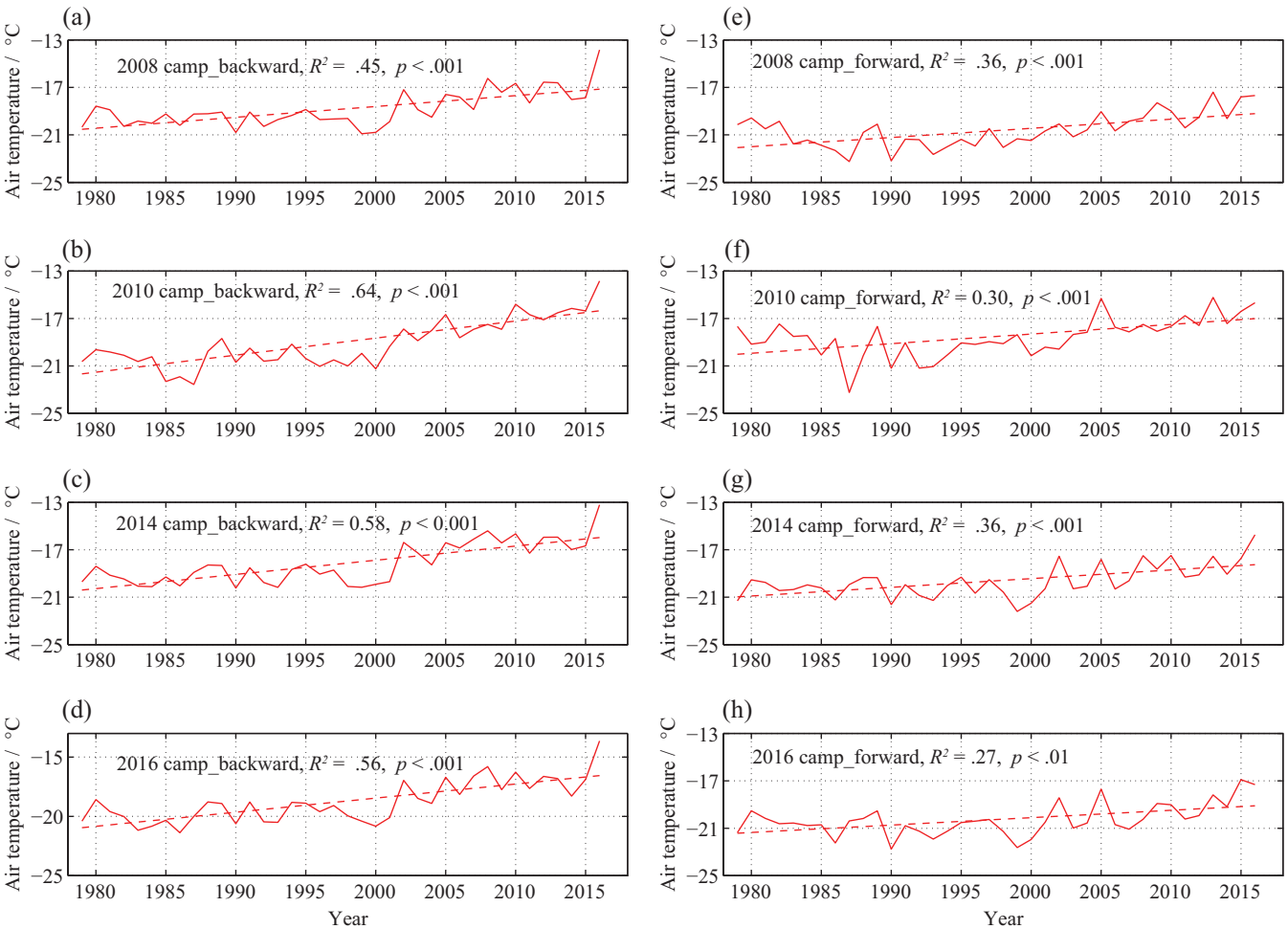

FIGURE 7 Long-term changes in average SAT from 1 September to 6 June obtained along the fixed ice trajectories reconstructed in the operational year of buoys. The red dashed line shows the linear fit

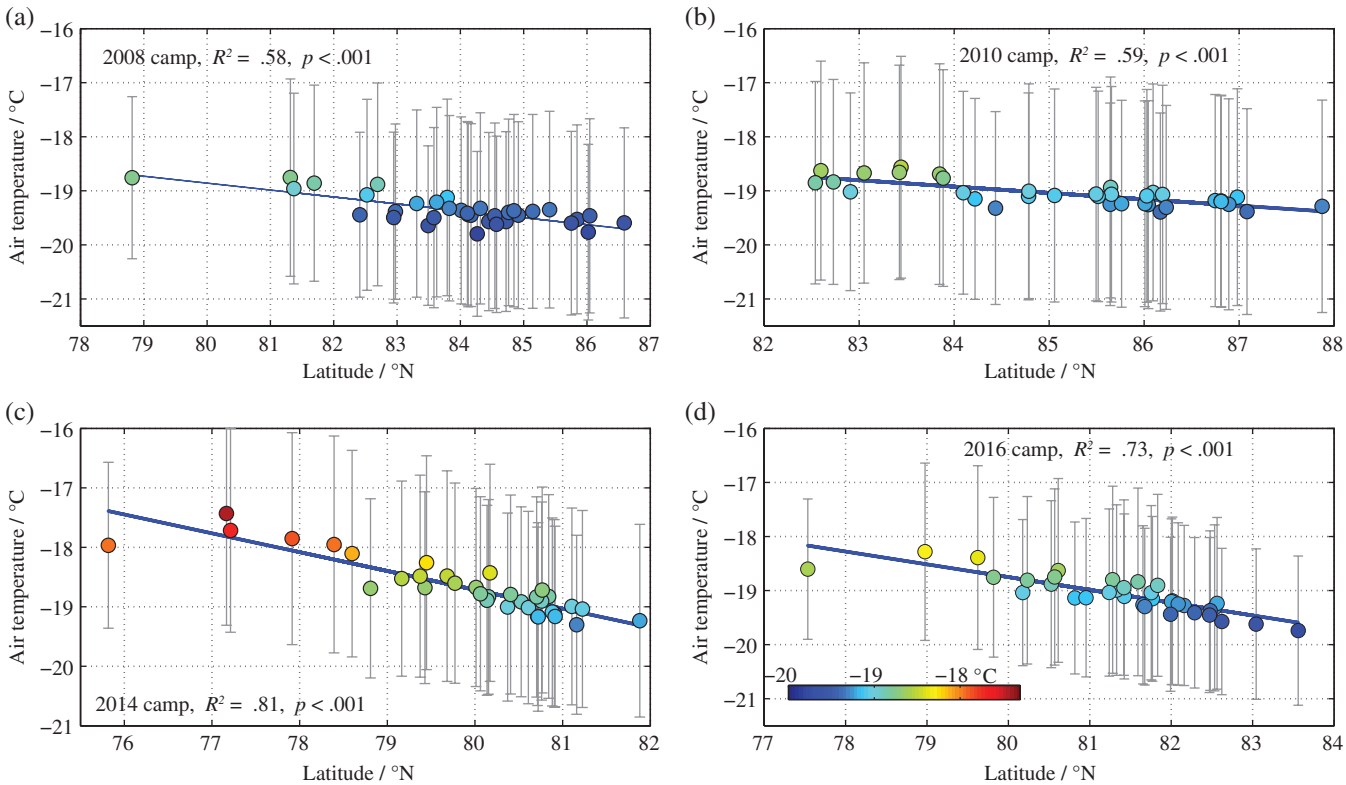

FIGURE 8 Variations in the average SAT from 1 September to 6 June obtained along the reconstructed backward trajectories in various years (1979–2016) against the average latitude of the trajectories. Filled circles and grey bars denote the long-term averages of 1979–2016 and their *SDs*, respectively, and the blue line shows the linear fit

the camps sites of 2008, 2010, 2014, and 2016, respectively. Although the correlation coefficients based on the detrended data were slightly smaller than those based on the raw data, they were still significant at the 99.9% level. This further indicates that the influence of the intensity of the TDS on atmospheric thermodynamic forcing for sea ice growth is physically meaningful.

3.3 | Change in ice concentration along ice trajectories

Along the September leg of the fixed backward trajectories, the linear regression (Figure 9) shows that September ice concentration decreased significantly from about 95% in 1979 to about 40% by 2016 for the 2008 and 2016 camp sites, and to about 20% for the 2014 camp site ($p < .001$). However, the corresponding decreased value was relatively small from 90 to 65% during 1979–2016 for the 2010 camp ($p < .05$) because of its relative high latitude of the backward trajectories compared to other camp sites. Sea ice originating from low latitudes has tended to experience lower-concentration ice conditions during early autumn in recent years, which, associated with the increased melt pond coverage over the ice (Rösel and Kaleschke, 2012), would have led to increased absorption of solar radiation by the upper ocean. We assumed constant values of the transmittance ratio of solar radiation for both ice cover (0.04) and open water (0.93) using typical observed values of multiyear ice (Nicolaus et al., 2012) and leads (Pegau and Paulson, 2001). Thus, a decrease in ice concentration from 95 to 20% could lead to an increase from 0.09 to 0.75 in the composite transmittance of solar radiation into the upper ocean. This would increase oceanic heat flux under the ice and result in delayed onset of basal ice freezing.

Along the backward trajectories reconstructed in various years, the September ice concentration along the September legs was found to be significantly dependent on the latitude of trajectory (Figure 10). This implies the influence of the TDS on sea ice thermodynamic processes. Specifically, an enhanced TDS would advect more ice from low latitudes, with most from the Chukchi and East Siberian seas (Figure 2), where ice conditions would be conducive to increased input of solar heat into the ice–ocean system. For the 2014 and 2016 camps, the September ice concentration obtained from the backward trajectories in the 2007/08 ice season deviated significantly (by more than two *SDs* of the regression error) from the linear regression of ice concentration against latitude. This was because the September legs of the backward trajectories in this year were located in the eastern BG region close to Banks Island (Figure 2c,d), where

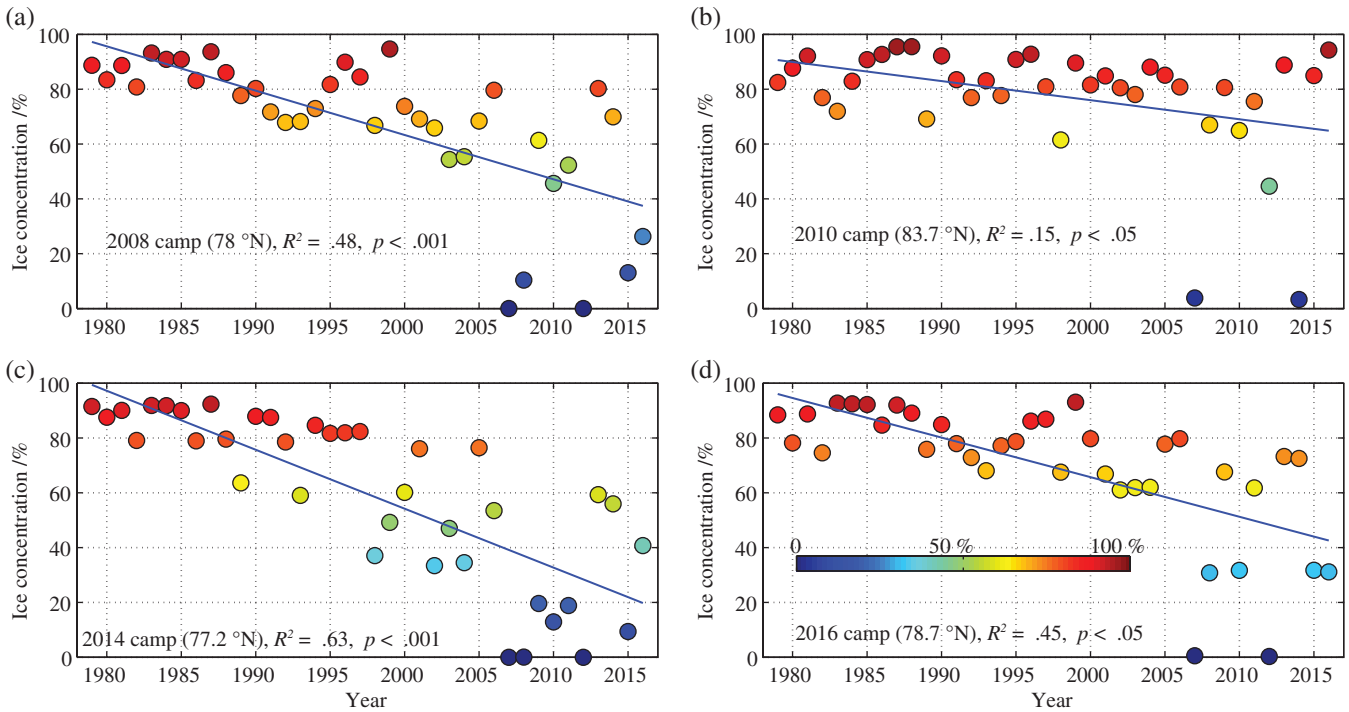

FIGURE 9 Long-term change in September ice concentration along backward trajectories reconstructed in the operational years of the camps. Also shown are linear fits (blue lines) and their correlation coefficients and confidence levels, as well as the average latitude of the September trajectories

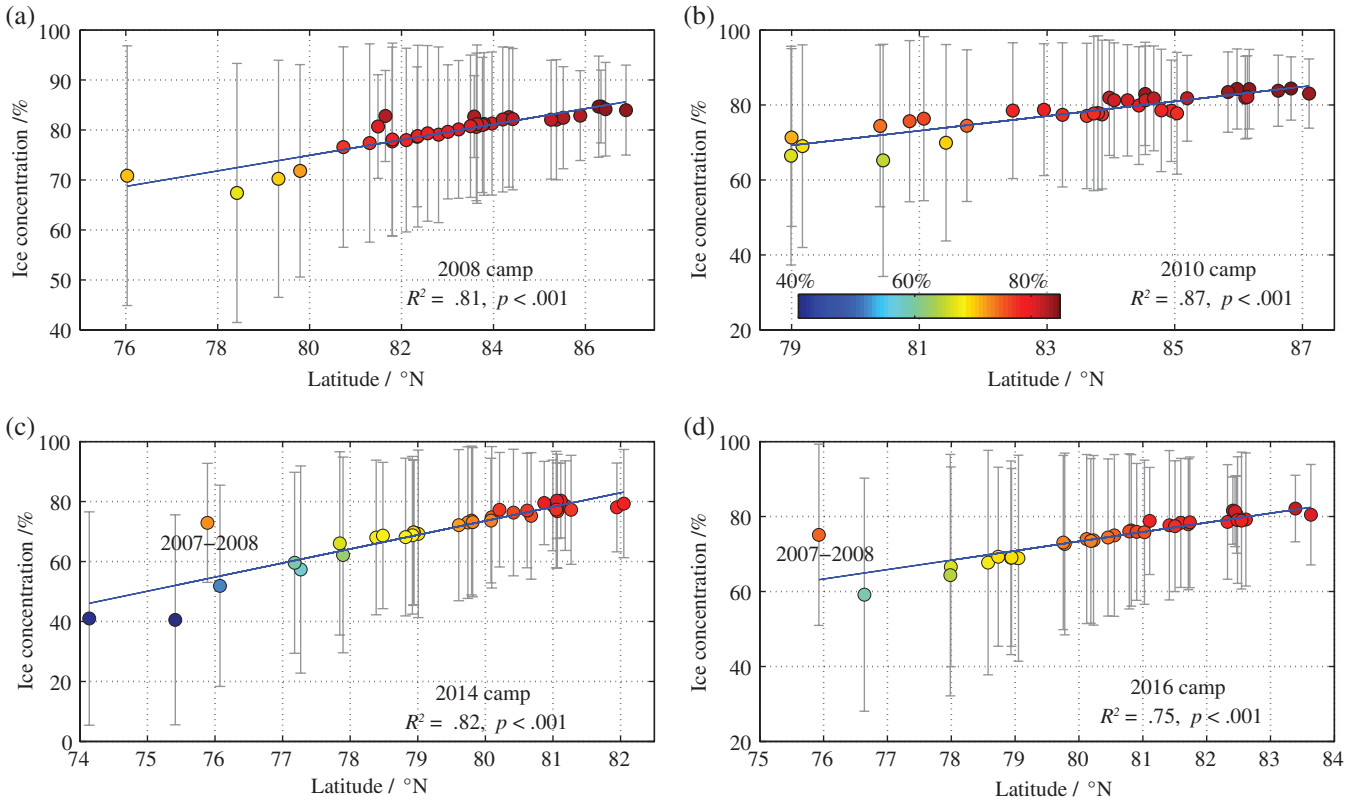

FIGURE 10 Variations in average September ice concentration obtained along the backward ice trajectories against the average September latitude of the trajectories. The scatter and grey bars denote the averages and *SDs* for 1979–2016. Blue line shows the linear fit

the ice concentration was generally larger than that at the same latitude in the Chukchi and East Siberian seas. The *SD* for the ice concentration obtained from the various years decreased strongly from south to north. This was because higher latitudes will in general have higher sea–ice concentrations, and hence the range of variability would be expected to be smaller. We also recalculated the regressions based on the detrended ice concentration and latitude in September. The squared correlation coefficients based on the detrended data were 0.78, 0.73, 0.80, and 0.73, for the camp sites of 2008, 2010, 2014, and 2016, respectively, all of which were very close to those obtained using the raw data and significant at the 99.9% level. This increased our confidence on the results revealed using the raw data. For example, the detrended September ice concentration in the 2007/08 ice season also deviated significantly from the regression by more than two *SDs*.

4 | DISCUSSION

4.1 | Uncertainties of the reconstructed ice drift trajectories

To investigate the influence of the accuracy of remote sensing ice motion products on the estimation of sea ice trajectories, we compared the distances between the positions measured by the buoys deployed at the ice camps and drift estimated using the NSIDC and OSI-SAF remote sensing products (OSI-405-b). We note that our buoy data have not been assimilated in any ice motion product. The OSI-SAF ice motion vectors with a time span of 48 hr are estimated using a continuous maximum cross-correlation method on pairs of satellite images (Lavergne and Eastwood, 2010). Because the OSI-SAF data were available only for the freezing season from October to April, the comparison focuses on this period using the starting positions measured by the buoys on 1 October. Starting from the positions of the 2008 and 2010 camps on 1 October, the distance between the buoy position and the position estimated using the NSIDC data was found to be comparable with that between the buoy position and the position estimated using the OSI-SAF data until late January, both of which have values smaller than 70 km (Figure 11). From then onward, the NSIDC-estimated position started to deviate further from the camp position in comparison with the OSI-SAF position. Especially for the 2010 camp, the distance between the camp position and the NSIDC-estimated position increased rapidly from about 70 km at the beginning of March to about 250 km by the end of April 2011 when the ice camp was advected toward Fram Strait. The 10-year average distance during 2005–2015 between the two estimated positions increased nearly linearly from autumn to the following spring. By the end of April, the average distance in relation to the position of the 2008 camp increased to 103 ± 83 km. Here, it should be noted that the distance corresponding to the 2010 camp could not be calculated after mid-February for 6 years

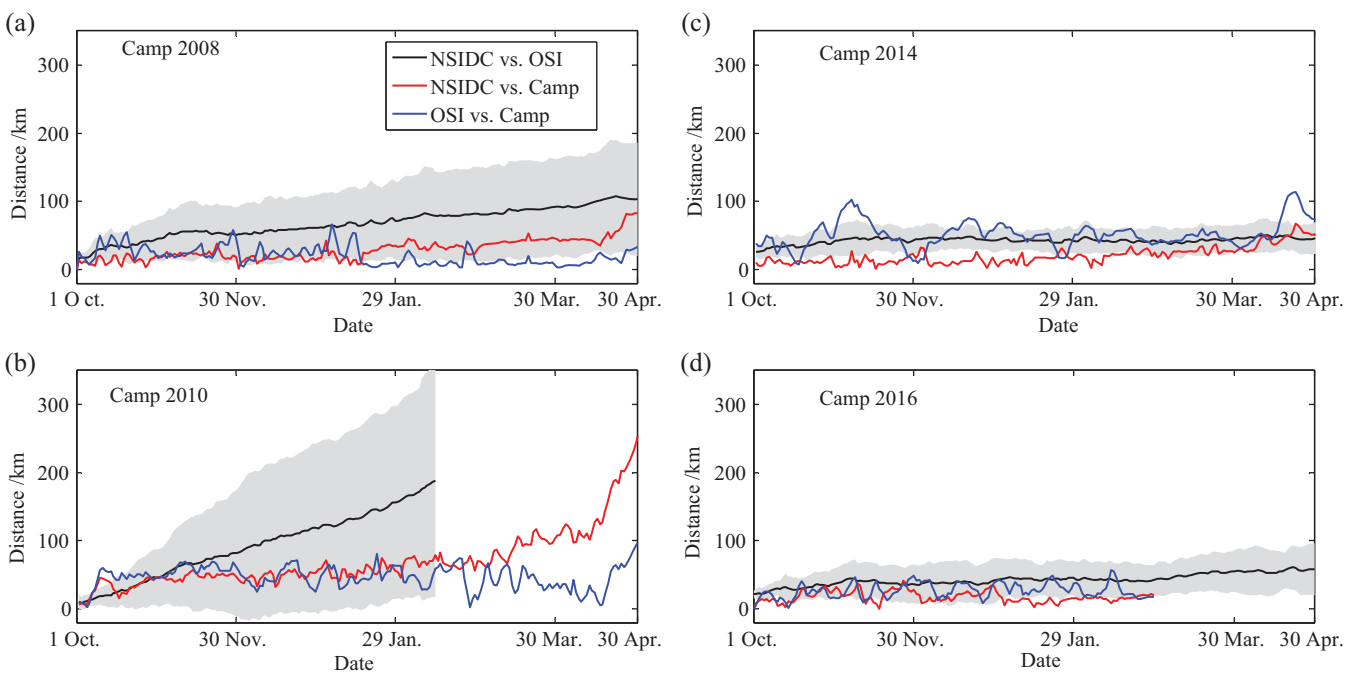

FIGURE 11 Distance between camp position measured by the buoy and the position estimated using the NSIDC (red line) or OSI-SAF (blue line) remote sensing products in the operational year of the buoy, and the average (±*SD*) distance in 2005–2015 (black line and grey shading) between the positions estimated using the NSIDC and OSI-SAF remote sensing products

during 2005–2015 because there were gaps in the OSI-SAF data when the floes were advected into the MIZ. By mid-February, the average distance increased to about 170 ± 150 km in relation to the position of this camp. Thus, the NSIDC data have weaker skill to reproduce ice motion in the downstream region of TDS compared with OSI-SAF data, especially in the region close to Fram Strait. However, the gaps in OSI-SAF data in the MIZ, attributable to low ice concentrations, also limit the applicability of these data to the reconstruction of ice trajectories.

In contrast, for the 2014 and 2016 camps, the distance between the estimated positions and the buoy position, and that between the estimated positions obtained from the two remote sensed products remained <100 km. This implies that both remote sensed products can reproduce the BG motion better than drift in the downstream region of TDS, and that the differences between two remote sensed products are not spatially uniform. This is likely attributable to the lower ice speed and the larger ice concentration in the BG region in comparison with the region close to Fram Strait. Both factors would lead to decreased uncertainty of the remote sensed ice motion products (Hwang, 2013; Sumata et al., 2014). Nevertheless, we suggest that NSIDC data are adequate for use in determining the terminal positions of the trajectories for ice advected from the camp deployment sites, because the data uncertainty remained reasonable when the ice floe drifted into the intersection region between the northeast of BG system and the downstream of TDS. Consequentially, the general direction of ice motion (toward the BG region or the TDS region) can still be clearly identified.

4.2 | Representativeness of the original positions of the reconstructed ice drift trajectories

In this study, we set the original positions at four deployment sites of ice camps to reconstruct the backward and forward ice drift trajectories. It is convenient to validate the reconstructed ice trajectories using the buoy data. However, this also raises questions about the representativeness of the defined positions because of the randomness of the camp deployment. To assess the representativeness of the defined positions, we reconstructed the backward and forward ice trajectories from 1979 to 2016 for 16 sites in a region of about 900 km × 500 km surrounding the camp sites, which also in the boundary region between the BG and the TDS. Firstly, we compared the forward ice trajectories from 20 sites, including the camp sites and the 16 other test sites, in four ice seasons of 2002/03, 2003/04, 2007/08, and 2012/13, which were selected because of their abnormal (larger or smaller than one *SD* related to 1979–2016 average) BH and CAI. In ice seasons 2002/03 and 2007/08, the annual (September to follow August) CAI was abnormal high, with the values of 3.4 and 4.2 hPa, respectively. Such pattern of atmospheric circulation is conducive to the advection of ice floes from most test positions to the downstream TDS system, as shown in Figure 12a,c. Furthermore, the forward ice trajectories show a cyclonic (anticyclonic) trend in the ice season of 2002/03 (2007/08) because of the abnormal low (high) winter BH anomaly with a value of –10.8 hPa (9.0 hPa). Thus, there were no ice floes advected distinctly into the BG system in 2002/03, while three from the southeast corner of the study region advected into the BG system in 2007/08. In contrast, the annual CAI was abnormal low, with the values of –0.8 and 0.5 hPa in the ice seasons of 2003/04 and 2012/13, respectively. Thus, there were no ice floes from the study region advected into the TDS system during both ice seasons. Especially in 2012/2013, all the ice floes were advected southwestward because of the abnormal high (10.4 hPa) winter BH anomaly. The abnormal low CAI occurring in all seasons in 2012/13 only with a mild exception in spring 2013, which resulted in an extremely weak sea ice outflow from the Arctic Ocean to Fram Strait throughout this year and consequently a marked recovery for the Arctic sea ice extent in September 2013, with annual minimum value of 5.10×10^6 km^2, which exceeded that in September 2012 by about 50% (Wang et al., 2016).

Secondly, we performed the correlation analysis between the annual CAI or the winter BH anomaly and the difference in latitude of the backward trajectories or in longitude of the forward trajectories. Here, we used the difference in latitude/longitude, but not the latitude/longitude of terminal points, because the 20 test sites had a relatively large range in the original latitude/longitude. From comparison among the 20 test sites, we found that, the squared correlation coefficients obtained from the camp sites were close to those obtained from other test sites, and all the correlations shown in Figure 13 were significantly at the 95% level. For all test sites, the explained degree (R^2) of the annual average CAI for the variance of the difference in latitude from the original position to the terminal position of the backward trajectories is significant at the 99.9% level, which is more significant than that for the variance of the difference in longitude of the forward trajectories. This indicates the influence of the TDS on the backward trajectories was stronger than on the forward trajectories. Furthermore, the explained degree of the variance of the difference in longitude of the forward trajectories by the annual average CAI was more significant than by the winter BH anomaly, especially for the sites in the north. This implies the forward trajectories were more affected by the strength of TDS than by the strength of winter BG. The above statistical conclusions are consistent for both the camp sites and the other test sites. Thus, we can infer that the regulation mechanism of atmospheric

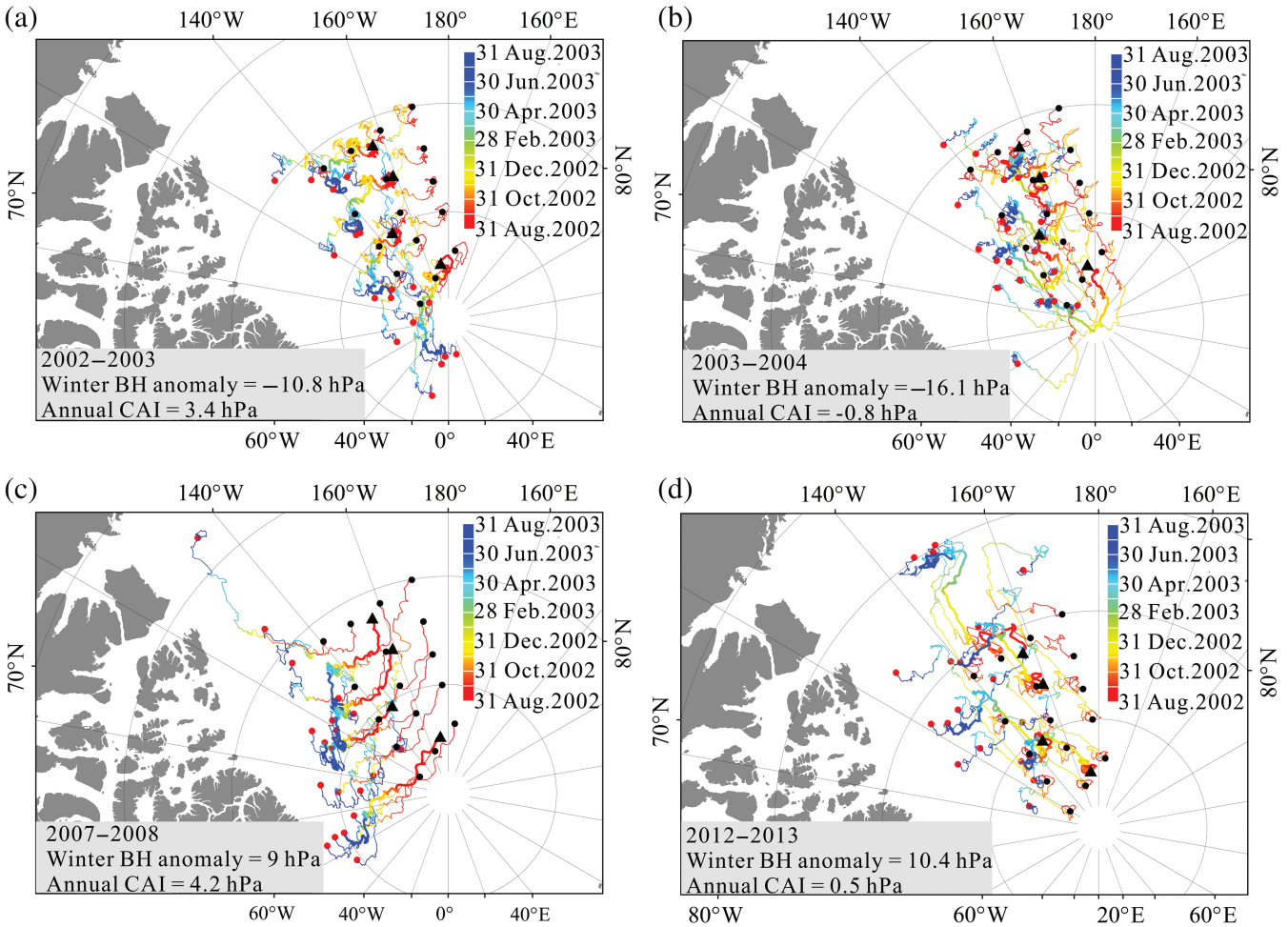

FIGURE 12 The reconstructed forward ice drift trajectories originated from 20 sites in a wide region centred at the camp sites during four ice seasons. The black and red dots denote the start and terminal positions of the ice trajectories, and the black triangles denote the deployment sites of four ice camps. The values of winter BH anomaly and annual CAI are shown in each panel

circulations on sea ice movement identified from the reconstructed backward or forward ice trajectories originated from four camps is also suitable for a wide boundary region between the BG and the TDS.

5 | CONCLUDING REMARKS

The NSIDC remote sensed ice motion product was used to reconstruct backward and forward drifting trajectories from four camps established in the summers of 2008, 2010, 2014, and 2016. These camps were located in a region where ice drift can oscillate between motion in the BG or the TDS. Based on comparisons with buoy measurements and the OSI-SAF remote sensed product, we found the NSIDC product has sufficient capability to estimate the original and terminal positions of the backward and forward trajectories, although it underestimates the southward speed of motion when ice is advected into Fram Strait.

From the reconstructed backward and forward ice trajectories during 1979–2016, the original positions of all the camp sites were found to show significant tendency of increasing advection from lower latitudes in recent years. The floes from all the camps were advected to lower-longitude regions and became more involved in the downstream of TDS system in recent years. An enhanced TDS would advect more ice from the lower latitudes of the Laptev, East Siberian, and Chukchi seas into the central Arctic Ocean, promoting the retreat of sea ice during summer in these peripheral seas of the Arctic. This mechanism also would enhance the ice-based material transport from Arctic shelf regions to the Arctic basin region. Furthermore, an enhanced TDS would play a crucial role in sea ice loss for the entire Arctic Ocean via the export of sea ice from the central Arctic Ocean into the Greenland Sea or the Barents Sea, where the ice would melt even in winter.

The original positions of the backward ice trajectories and the terminal positions of the forward ice trajectories were significantly related to the atmospheric circulation

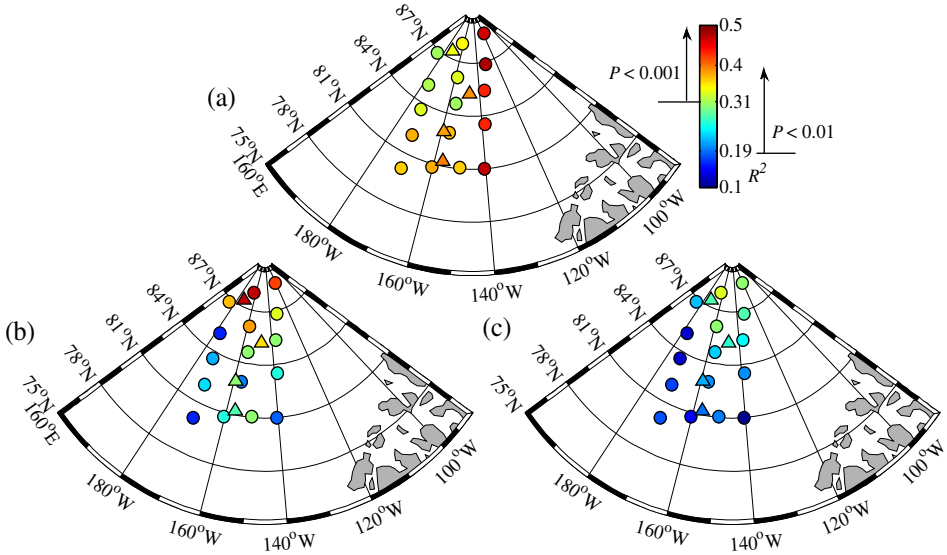

FIGURE 13 The squared correlation coefficients (a) between the difference in latitude from the original position to the terminal position of the reconstructed backward trajectories and the annual average CAI, (b) between the difference in longitude from the original position to the terminal position of the reconstructed forward trajectories and the annual average CAI, and (c) between the difference in longitude from the original position to the terminal position of the reconstructed forward trajectories and the winter BH anomaly, with the triangles denoting the four camp sites and circles denoting the other test sites as shown in Figure 12

pattern. Generally, the CAI has better skill than the DA index in explaining the original and terminal positions of the backward or forward trajectories. The squared correlation coefficient (R^2) between the seasonal DA and CAI for the period of 1979–2016 was in the range 0.46–0.86, all of which were significant at the 99.9% level. This indicates both indices are related to similar patterns in nature. However, the DA index cannot indicate the orientation of the Arctic SLP dipole. The CAI is calculated across the TDS region, thus it can depict an east–west dipole pattern of SLP perpendicular to the TDS and can be closer related to the ice motion along the TDS compared to the DA index. Compared with the AO index, the BH anomaly has better skill in explaining the terminal positions of the forward trajectories. This is because the AO index characterizes the pan-Arctic atmospheric circulation north of 70°N, whereas the BH anomaly characterizes the atmospheric circulation over the western Arctic Ocean, which is related closely to the curl of surface wind stress and sea ice motion in this region. Under the scenario of an abnormal high BH anomaly, ice floes from the camps would tend to become trapped within a region close to the North Pole or they would drift into the BG region, which would restrict the advection of ice toward the Fram Strait. Thereby, such a situation is not conducive to the loss of sea ice over the Arctic Ocean. However, an abnormal high BH anomaly is conducive to the retreat of summer sea ice for the lower-latitude region of western Arctic through inducing anomalous Ekman drift of sea ice from the Beaufort, Chukchi, and East Siberian seas toward the central Arctic (Ogi et al., 2008).

During the freezing season, Arctic climate warming and the poleward gradient of SAT were found more significant than in the melt season. The melting of Arctic sea ice can damp an atmospheric climate warming signal in summer. The delayed surface freeze-up identified by satellite passive microwave observation is mainly attributed to the ice-albedo feedback and the wind-wave driven ice fracture and ocean vertical mixing, but not the change in SAT during autumn because no significant delayed trend has been identified for the onset of freeze-up point based on the SAT. The onset of basal freezing of sea ice at low latitudes is likely to have greater delay compared with the high-latitude pack ice zone. This is because low-latitude oceans absorb more solar radiation and they experience stronger positive ice–albedo feedback and wind-derived waves.

ACKNOWLEDGEMENTS

The SMMR-SSMIS ice concentration data were provided by the National Snow and Ice Data Center (NSIDC). Ice motion products were provided by the NSIDC and Ocean and Sea Ice Satellite Application Facility. The atmospheric reanalysis data were obtained from the European Centre for Medium-Range Weather Forecasts and the National Centers for Environmental Prediction/National Center for Atmospheric Research.

This work was supported by the National Key R&D Program of China (2018YFA0605903 & 2016YFC14003) and the National Natural Science Foundation of China (41722605). J.H. was supported by the U.S.A. National

Science Foundation grants OPP1722729 and OPP1740768. J.W. was supported by NOAA CPO Office of Arctic Research. Three anonymous reviewers are greatly thanked for their constructive reviews.

ORCID

Ruibo Lei https://orcid.org/0000-0001-8525-8622

REFERENCES

Asplin, M.G., Lukovich, J.V. and Barber, D.G. (2009) Atmospheric forcing of the Beaufort Sea ice gyre: surface pressure climatology and sea ice motion. *Journal of Geophysical Research*, 114, C00A06. https://doi.org/10.1029/2008JC005127.

Asplin, M.G., Galley, R., Barber, D.G. and Prinsenberg, S. (2012) Fracture of summer perennial sea ice by ocean swell as a result of Arctic storms. *Journal of Geophysical Research*, 117, C06025. https://doi.org/10.1029/2011JC007221.

Asplin, M.G., Scharien, R., Else, B., Howell, S., Barber, D.G., Papakyriakou, T. and Prinsenberg, S. (2014) Implications of fractured Arctic perennial ice cover on thermodynamic and dynamic sea ice processes. *Journal of Geophysical Research*, 119, 2327–2343. https://doi.org/10.1002/2013JC009557.

Chylek, P., Folland, C.K., Lesins, G., Dubey, M.K. and Wang, M. (2009) Arctic air temperature change amplification and the Atlantic Multidecadal Oscillation. *Geophysical Research Letters*, 36, L14801. https://doi.org/10.1029/2009GL038777.

Dee, D.P., et al. (2011) The ERA-interim reanalysis: configuration and performance of the data assimilation system. *Quarterly Journal of the Royal Meteorological Society*, 137, 553–597. https://doi.org/10.1002/qj.828.

Girard-Ardhuin, F. and Ezraty, R. (2012) Enhanced Arctic sea ice drift estimation merging radiometer and scatterometer data. *IEEE Transactions on Geoscience and Remote Sensing*, 50(7), 2639–2648. https://doi.org/10.1109/TGRS.2012.2184124.

Graham, R.M., Cohen, L., Petty, A.A., Boisvert, L.N., Rinke, A., Hudson, S.R., Nicolaus, M. and Granskog, M.A. (2017) Increasing frequency and duration of Arctic winter warming events. *Geophysical Research Letters*, 44, 6974–6983. https://doi.org/10.1002/2017GL073395.

Hutter, N., Losch, M. and Menemenlis, D. (2018) Scaling properties of arctic sea ice deformation in a high-resolution viscous-plastic sea ice model and in satellite observations. *Journal of Geophysical Research, Oceans*, 123, 672–687. https://doi.org/10.1002/2017JC013119.

Hwang, B. (2013) Inter-comparison of satellite sea ice motion with drifting buoy data. *International Journal of Remote Sensing*, 34 (24), 8741–8763.

Kalnay, E., Kanamitsu, M., Kistler, R., Collins, W., Deaven, D., Gandin, L., Iredell, M., Saha, S., White, G., Woollen, J., Zhu, Y., Leetmaa, A., Reynolds, R., Chelliah, M., Ebisuzaki, W., Higgins, W., Janowiak, J., Mo, K.C., Ropelewski, C., Wang, J., Jenne, R. and Joseph, D. (1996) The NCEP/NCAR 40-year reanalysis project. *Bulletin of the American Meteorological Society*, 77(3), 437–471. https://doi.org/10.1175/1520-0477(1996)077<0437:TNYRP>2.0.CO;2.

Kwok, R., Spreen, G. and Pang, S. (2013) Arctic sea ice circulation and drift speed: decadal trends and ocean currents. *Journal of Geophysical Research, Oceans*, 118, 2408–2425.

Kimura, N., Nishimura, A., Tanaka, Y. and Yamaguchi, H. (2013) Influence of winter sea ice motion on summer ice cover in the Arctic. *Polar Research*, 32, 20193. https://doi.org/10.3402/polar.v32i0.20193.

Langehaug, H.R., Geyer, F., Smedsrud, L.H. and Gao, Y. (2013) Arctic sea ice decline and ice export in the CMIP5 historical simulations. *Ocean Modelling*, 71, 114–126.

Lavergne T, Eastwood S. 2010. Low Resolution Sea Ice Drift Product User's Manual, GBL LR SID-OSI 405, the EUMETSAT Network of Satellite Appl. Fac.

Lee, S., Gong, T., Feldstein, S.B., Screen, J.A. and Simmonds, I. (2017) Revisiting the cause of the 1989-2009 Arctic surface warming using the surface energy budget: downward infrared radiation dominates the surface fluxes. *Geophysical Research Letters*, 44(20), 10654–10661. https://doi.org/10.1002/2017GL075375.

Lei, R., Xie, H., Wang, J., Leppäranta, M., Jónsdóttir, I. and Zhang, Z. (2015) Changes in sea ice conditions along the Arctic Northeast Passage from 1979 to 2012. *Cold Regions Science and Technology*, 119, 132–144.

Lei, R., Tian-Kunze, X., Leppäranta, M., Wang, J., Kaleschke, L. and Zhang, Z. (2016) Changes in summer sea ice, albedo, and portioning of surface solar radiation in the Pacific sector of Arctic Ocean during 1982–2009. *Journal of Geophysical Research, Oceans*, 121, 5470–5486. https://doi.org/10.1002/2016JC011831.

Lei, R., Cheng, B., Heil, P., Vihma, T., Wang, J., Ji, Q. and Zhang, Z. (2018) Seasonal and interannual variations of sea ice mass balance from the Central Arctic to the Greenland Sea. *Journal of Geophysical Research, Oceans*, 123, 2422–2439. https://doi.org/10.1002/2017JC013548.

Lindsay, R. and Schweiger, A. (2015) Arctic sea ice thickness loss determined using subsurface, aircraft, and satellite observations. *The Cryosphere*, 9, 269–283.

Lukovich, J.V. and Barber, D.G. (2006) Atmospheric controls on sea ice motion in the southern Beaufort Sea. *Journal of Geophysical Research*, 111, D18103. https://doi.org/10.1029/2005JD006408.

Markus, T. and Cavalieri, D.J. (2000) An enhancement of the NASA team sea ice algorithm. *IEEE Transactions on Geoscience and Remote Sensing*, 38(3), 1387–1398.

Moore, G.W.K., Schweiger, A., Zhang, J. and Steele, M. (2018) Collapse of the 2017 winter Beaufort High: a response to thinning sea ice? *Geophysical Research Letters*, 45, 2860–2869. https://doi.org/10.1002/2017GL076446.

Nicolaus, M., Katlein, C., Maslanik, J. and Hendricks, S. (2012) Changes in Arctic sea ice result in increasing light transmittance and absorption. *Geophysical Research Letters*, 39, L24501. https://doi.org/10.1029/2012GL053738.

Ogi, M., Rigor, I.G., McPhee, M.G. and Wallace, J.M. (2008) Summer retreat of Arctic sea ice: role of summer winds. *Geophysical Research Letters*, 35, L24701. https://doi.org/10.1029/2008GL035672.

Ogi, M., Yamazaki, K. and Wallace, J.M. (2010) Influence of winter and summer surface wind anomalies on summer Arctic sea ice extent. *Geophysical Research Letters*, 37, L07701. https://doi.org/10.1029/2009GL042356.

Overland, J.E. (2009) Meteorology of the Beaufort Sea. *Journal of Geophysical Research*, 114, C00A07. https://doi.org/10.1029/2008JC004861.

Overland, J.E., Francis, J.A., Hanna, E. and Wang, M. (2012) The recent shift in early summer Arctic atmospheric circulation. *Geophysical Research Letters*, 39, L19804. https://doi.org/10.1029/2012GL053268.

Parkinson, C.L. and Comiso, J.C. (2013) On the 2012 record low Arctic sea ice cover: combined impact of preconditioning and an August storm. *Geophysical Research Letters*, 40, 1356–1361. https://doi.org/10.1002/grl.50349.

Parkinson, C.L. (2014) Spatially mapped reductions in the length of the Arctic sea ice season. *Geophysical Research Letters*, 41, 4316–4322. https://doi.org/10.1002/2014GL060434.

Peeken, I., Primpke, S., Beyer, B., Gutermann, J., Katlein, C., Krumpen, T., Bergmann, M., Hehemann, L. and Gerdts, G. (2018) Arctic sea ice is an important temporal sink and means of transport for microplastic. *Nature Communications*, 9, 1050. https://doi.org/10.1038/s41467-018-03825-5.

Perovich, D.K., Light, B., Eicken, H., Jones, K.F., Runciman, K. and Nghiem, S.V. (2007) Increasing solar heating of the Arctic Ocean and adjacent seas, 1979–2005: attribution and role in the ice-albedo feedback. *Geophysical Research Letters*, 34, L19505. https://doi.org/10.1029/2007GL031480.

Pegau, W.S. and Paulson, C.A. (2001) The albedo of Arctic leads in summer. *Annals of Glaciology*, 33, 221–224.

Petty, A.A., Hutchings, J.K., Richter-Menge, J.A. and Tschudi, M.A. (2016) Sea ice circulation around the Beaufort Gyre: the changing role of wind forcing and the sea ice state. *Journal of Geophysical Research, Oceans*, 121, 3278–3296. https://doi.org/10.1002/2015JC010903.

Petty, A.A. (2018) A possible link between winter Arctic sea ice decline and a collapse of the Beaufort High? *Geophysical Research Letters*, 45, 2879–2882. https://doi.org/10.1002/2018GL077704.

Petty, A.A., Stroeve, J.C., Holland, P.R., Boisvert, L.N., Bliss, A.C., Kiumar, N. and Meier, W.N. (2018) The Arctic sea ice cover of 2016: a year of record-low highs and higher-than-expected lows. *The Cryosphere*, 12, 433–452.

Proshutinsky, A.Y. and Johnson, M.A. (1997) Two circulation regimes of the wind-driven Arctic Ocean. *Journal of Geophysical Research, Oceans*, 102, 12493–12514.

Proshutinsky, A.Y., et al. (2009) Beaufort Gyre freshwater reservoir: state and variability from observations. *Journal of Geophysical Research, Oceans*, 114, C00A10. https://doi.org/10.1029/2008JC005104.

Rainville, L. and Woodgate, R.A. (2009) Observations of internal wave generation in the seasonally ice-free Arctic. *Geophysical Research Letters*, 36, L23604. https://doi.org/10.1029/2009GL041291.

Rösel, A. and Kaleschke, L. (2012) Exceptional melt pond occurrence in the years 2007 and 2011 on the Arctic sea ice revealed from MODIS satellite data. *Journal of Geophysical Research*, 117, C05018. https://doi.org/10.1029/2011JC007869.

Richter-Menge, J.A., Perovich, D.K., Elder, B.C., Claffey, K., Rigor, I. and Ortmeyer, M. (2006) Ice mass balance buoys: a tool for measuring and attributing changes in the thickness of the Arctic sea-ice cover. *Annals of Glaciology*, 44, 205–210.

Rudeva, I. and Simmonds, I. (2015) Variability and trends of global atmospheric frontal activity and links with large-scale modes of variability. *Journal of Climate*, 28(8), 3311–3330.

Screen, J. and Simmonds, I. (2010) The central role of diminishing sea ice in recent Arctic temperature amplification. *Nature*, 464(7293), 1334–1337.

Screen, J.A., Bracegirdle, T.J. and Simmonds, I. (2018) Polar climate change as manifest in atmospheric circulation. *Current Climate Change Reports*, 4, 383–395. https://doi.org/10.1007/s40641-018-0111-4.

Simmonds, I., Burke, C. and Keay, K. (2008) Arctic climate change as manifest in cyclone behavior. *Journal of Climate*, 21(22), 5777–5796. https://doi.org/10.1175/2008JCLI2366.1.

Simmonds, I. and Keay, K. (2009) Extraordinary September Arctic sea ice reductions and their relationships with storm behavior over 1979–2008. *Geophysical Research Letters*, 36, L19715. https://doi.org/10.1029/2009GL039810.

Simmonds, I. (2015) Comparing and contrasting the behavior of Arctic and Antarctic sea ice over the 35 year period 1979–2013. *Annals of Glaciology*, 56(69), 18–28.

Šmejkalová, T., Edwards, M.E. and Dash, J. (2016) Arctic lakes show strong decadal trend in earlier spring ice-out. *Scientific Reports*, 6 (1), 38449. https://doi.org/10.1038/srep38449.

Sotiropoulou, G., Tjernström, M., Sedlar, J., Achtert, P., Brooks, B.J., Brooks, I.M., Persson, P.O., Prytherch, J., Salisabury, D.J., Shupe, M.D., Johnston, P.E. and Wolfe, D. (2016) Atmospheric conditions during the Arctic clouds in summer experiment (ACSE): contrasting open water and sea ice surfaces during melt and freeze-up seasons. *Journal of Climate*, 29(24), 8721–8744. https://doi.org/10.1175/JCLI-D-16-0211.1.

Spreen, G., Kwok, R. and Menemenlis, D. (2011) Trends in Arctic sea ice drift and role of wind forcing: 1992–2009. *Geophysical Research Letters*, 38, L19501. https://doi.org/10.1029/2011GL048970.

Strong, C. and Rigor, I.G. (2013) Arctic marginal ice zone trending wider in summer and narrower in winter. *Geophysical Research Letters*, 40, 4864–4868. https://doi.org/10.1002/grl.50928.

Stroeve, J.C., Markus, T., Boisvert, L., Miller, J. and Barrett, A. (2014) Changes in Arctic melt season and implications for sea ice loss. *Geophysical Research Letters*, 41, 1216–1225. https://doi.org/10.1002/2013GL05895.1.

Sumata, H., Lavergne, T., Girard-Ardhuin, F., Kimura, N., Tschudi, M. A., Kauker, F., Karcher, M. and Gerdes, R. (2014) An intercomparison of Arctic ice drift products to deduce uncertainty estimates. *Journal of Geophysical Research, Oceans*, 119(8), 4887–4921. https://doi.org/10.1002/2013JC009724.

Timco GW, Johnston ME. 2002. Sea ice strength during the melt season. *Proceedings of the 16th IAHR International Symposium on Ice. Vol. 2.* Dunedin, New Zealand; pp. 187–193.

Thomson, J. and Rogers, W.E. (2014) Swell and sea in the emerging Arctic Ocean. *Geophysical Research Letters*, 41, 3136–3140. https://doi.org/10.1002/2014GL059983.

Tremblay, L.B. and Mysak, L.A. (1997) Modeling sea ice as a granular material, including the dilatancy effect. *Journal of Physical Oceanography*, 27, 2342–2360.

Tschudi, M., Fowler, C., Maslanik, J., Stewart, J.S. and Meier, W. (2016) *Polar Pathfinder Daily 25 km EASE-Grid Sea Ice Motion Vectors, Version 3*. Boulder, CO: NASA National Snow and Ice Data Center Distributed Active Archive Center. https://doi.org/10.5067/O57VAIT2AYYY.

Tsukernik, M., Deser, C., Alexander, M. and Tomas, R. (2010) Atmospheric forcing of Fram Strait sea ice export: a closer look. *Climate*

Dynamics, 35, 1349–1360. https://doi.org/10.1007/s00382-009-0647-z.

Vihma, T., Tisler, P. and Uotila, P. (2012) Atmospheric forcing on the drift of Arctic sea ice in 1989–2009. *Geophysical Research Letters*, 39, L02501. https://doi.org/10.1029/2011GL050118.

Wang, C., Granskog, M.A., Hudson, S.R., Gerland, S., Pavlov, A.K., Perovich, D.K. and Nicolaus, M. (2016) Atmospheric conditions in the central Arctic Ocean through the melt seasons of 2012 and 2013: impact on surface conditions and solar energy deposition into the ice-ocean system. *Journal of Geophysical Research, Oceans*, 121, 1043–1058. https://doi.org/10.1002/2015JD023712.

Wang, J., Zhang, J., Watanabe, E., Mizobata, K., Ikeda, M., Walsh, J.E., Bai, X. and Wu, B. (2009) Is the Dipole Anomaly a major driver to record lows in the Arctic sea ice extent? *Geophysical Research Letters*, 36, L05706. https://doi.org/10.1029/2008GL036706.

Zhang, J., Lindsay, R., Schweiger, A. and Rigor, I. (2012) Recent changes in the dynamic properties of declining Arctic sea ice: a model study. *Geophysical Research Letters*, 39, L20503. https://doi.org/10.1029/2012GL053545.

How to cite this article: Lei R, Gui D, Hutchings JK, Wang J, Pang X. Backward and forward drift trajectories of sea ice in the northwestern Arctic Ocean in response to changing atmospheric circulation. *Int J Climatol*. 2019;1–20. https://doi.org/10.1002/joc.6080